THE ANATOMICAL RECORD 292:994–1027 (2009)

Architectonic Subdivisions of Neocortex in the Tree Shrew (*Tupaia belangeri*)

PEIYAN WONG AND JON H. KAAS*
Department of Psychology, Vanderbilt University, Nashville, Tennessee

ABSTRACT

Tree shrews are small mammals that bear some semblance to squirrels, but are actually close relatives of primates. Thus, they have been extensively studied as a model for the early stages of primate evolution. In this study, subdivisions of cortex were reconstructed from brain sections cut in the coronal, sagittal, or horizontal planes, and processed for parvalbumin, SMI-32-immunopositive neurofilament protein epitopes, vesicle glutamate transporter 2 (VGluT2), free ionic zinc, myelin, cytochrome oxidase, and Nissl substance. These different procedures revealed similar boundaries between areas, suggesting the detection of functionally relevant borders and allowed a more precise demarcation of cortical areal boundaries. Primary cortical areas were most clearly revealed by the zinc stain, because of the poor staining of layer 4, as thalamocortical terminations lack free ionic zinc. Area 17 (V1) was especially prominent, as the broad layer 4 was nearly free of zinc stain. However, this feature was less pronounced in primary auditory and somatosensory cortex. In primary sensory areas, thalamocortical terminations in layer 4 densely express VGluT2. Auditory cortex consists of two architectonically distinct subdivisions, a primary core region (Ac), surrounded by a belt region (Ab) that had a slightly less developed koniocellular appearance. Primary motor cortex (M1) was identified by the absence of VGluT2 staining in the poorly developed granular layer 4 and the presence of SMI-32-labeled pyramidal cells in layers 3 and 5. The presence of well-differentiated cortical areas in tree shrews indicates their usefulness in studies of cortical organization and function. Anat Rec, 292:994–1027, 2009. © 2009 Wiley-Liss, Inc.

Key words: rodents; primates; cortical areas; visual cortex; motor cortex; somatosensory cortex; auditory cortex; cingulate cortex; retrosplenial cortex; insular cortex

Abbreviations used: 3b(S1) = primary somatosensory area; Ab = auditory belt area; Ac = auditory core area; CB = calbindin; cc = corpus callosum; CGd = cingulate dorsal area; CGv = cingulate ventral area; Cl = claustral cortex; CO = cytochrome oxidase; DFC = dorsal frontal cortex; Ect = ectorhinal cortex; Ent = entorhinal cortex; EntI = entorhinal intermediate area; EntL = entorhinal lateral area; EntM = entorhinal medial area; Hippo = hippocampal cortex; HS = hippocampus supracommissuralis; Ins = insular cortex; IRd = infraradiata dorsalis; IRv = infraradiata ventral area; ITc = inferior temporal caudal area; ITi = inferior temporal intermediate area; ITr = inferior temporal rostral area; M1 = primary motor area; M2 = secondary motor area; MF = medial frontal cortex; MMA = medial motor area; MT = middle temporal visual area; OB = olfactory bulb; OFC = orbital frontal cortex; PB = phosphate buffer; PBS = phosphate buffer with saline; Pirf = piriform cortex; PPc = posterior parietal caudal area; PPd = posterior parietal dorsal area; PPr = posterior parietal rostral area; PRh = perirhinal area; PS = prostriata; PV = parvalbumin; Pv = parietal ventral area; Rsag = retrosplenial agranular area; RSg = retrosplenial granular area; S2 = secondary somatosensory area; SC = somatosensory caudal area; Sub = subiculum; TA = temporal anterior area; TD = temporal dorsal area; TI = temporal inferior area; TIV = temporal inferior ventral area; TP = temporal posterior area; TPI = temporal posterior inferior area; V1 = primary visual area; V2 = secondary visual area; VGluT2 = vesicle glutamate transporter 2.

Grant sponsor: National Eye Institute; Grant number: EY 02686.

*Correspondence to: Jon H. Kaas, Vanderbilt University, 301 Wilson Hall, 111 21st Avenue South, Nashville, TN 37203.
E-mail: jon.kaas@vanderbilt.edu

Received 9 January 2009; Accepted 12 March 2009

DOI 10.1002/ar.20916
Published online 19 May 2009 in Wiley InterScience (www.interscience.wiley.com).

The tree shrews are diurnal, arboreal mammals that bear some squirrel-like characteristics. At first glance, tree shrews and squirrels are so similar in appearance that to the natives in South-east Asia, they are one and the same animal, with both species bearing the same name Tupai in the Malay and Indonesian languages. In fact, when a Western naturalist, William Ellis, recorded the first tree shrew in 1780, he mistook it to be a squirrel. It took 40 years after the first recording before taxonomists recognized tree shrews as a separate species in the genus *Tupaia* (Emmons, 2000). Tree shrews are the only members of the order Scandentia that diversified from the rest of the Euarchontoglire clade about 85 million years ago (Murphy et al., 2001a; Huchon et al., 2002). Since then, tree shrews have been established as non-rodent, small mammals that, with flying lemurs, are the closest living relatives of primates (Liu et al., 2001; Murphy et al., 2001a,b; Springer et al., 2003). Tree shrews possess certain features of the brain that are shared with primates, such as a well-developed visual system and a reduced dependence on olfaction (Sorenson, 1970), and were once considered to be primates by Le Gros Clark (1959). Although this classification no longer holds, the observation made by Clark that tree shrews resemble primates, has resulted in tree shrews being the species of choice in many neuroanatomical and electrophysiological experiments. Here, we describe the architectonic subdivisions of neocortex in tree shrews, so as to establish a reliable areal cortical map that can be used to guide functional studies.

Tree shrews have often been used as animal models in the study of the visual system (e.g., Lund et al., 1985; Fitzpatrick, 1996). They are visually oriented animals with a retina consisting of mostly cones. The laterally placed eyes offer about 60-degree angle of binocular overlap (Kaas and Catania, 2002). The superior colliculus is exceptionally large compared with primates (Kaas and Huerta, 1988) and more distinctly laminated (Abplanalp, 1970; Lane et al., 1971). Their visual cortex is expansive. Primary visual cortex is relatively large and architectonically distinct, and several extrastriate visual areas have been proposed (Kaas et al., 1972; Sesma et al., 1984; Lyon et al., 1998). Pyramidal cells in primary visual cortex share a similar branching pattern to those found in primates, but are more branched and spinous than those found in galagos and monkeys (Elston et al., 2005). Primary visual cortex of tree shrews contains an orderly arrangement of orientation selective columns similar to those of primates (Humphrey and Norton, 1980; Bosking et al., 1997), whereas rodents do not (Van Hooser et al., 2005).

Given that tree shrews are arboreal and use their forepaws to climb and manipulate food items (Bishop, 1964), as do most primates, their sensorimotor system and cortex is well developed. Tree shrews are found to have at least five somatosensory fields, and a large forepaw representation is apparent in primary somatosensory cortex (Sur et al., 1980). The organization of the motor cortex has also been comprehensively characterized through corticospinal tracing and intracortical microstimulation, and the subdivisions of motor cortex have been defined cytoarchitecturally (Remple et al., 2006). There are two distinct motor fields that have been identified in tree shrews, and these areas have been found to share common features with the primary and premotor cortical areas of primates (Remple et al., 2006). The auditory cortex of tree shrews is less well studied. However, preliminary cortical mapping results indicate at least one auditory field, presumably the primary auditory cortex, which contains a complete tonotopic representation (Oliver and Hall, 1978). Architecturally, there are at least two definable regions in the auditory cortex of tree shrews. The first being a core region, which has a densely populated granular layer 4, and the second being a belt region, which has a less densely populated granular layer 4, located dorsal and medial to the core (Casseday et al., 1976).

These various studies reflect an interest in understanding the organization of tree shrew neocortex, and future studies may be better guided by a comprehensive architectonic map of tree shrew neocortex. There are three published architectonic maps of tree shrew neocortex to date. The first two were by Le Gros Clark (1924) and von Bonin and Bailey (1961), which showed only a few cortical areas. The third, by Zilles (1978), adopted a quantitative approach to determine the borders of cortical areas and defined a number of cortical areas. These earlier studies used the Nissl preparation to reveal cell bodies.

As the repertoire of staining procedures available has since increased, an update to the cortical maps is now timely. In this study, we use a battery of staining preparations to aid us in the characterization of cortical areas in the tree shrew. In addition to the traditional Nissl and myelin stains, another histochemical preparation, the zinc stain (Danscher, 1981, 1982; Danscher and Stoltenberg, 2005) has proved to be useful in revealing areal borders in the neocortex. This technique reveals free ionic zinc in the synapses of corticocortical terminations, allowing secondary sensory areas to be distinguished from primary sensory areas because the dense thalamocortical inputs in layer 4 of primary sensory areas lack free ionic zinc (e.g., Valente et al., 2002). Four immunohistochemical stains were also used, including those for neurofilaments (SMI-32), parvalbumin (PV), calbindin (CB), and the vesicle glutamate transporter 2 (VGluT2). The SMI-32 antibody reacts with nonphosphorylated epitopes in neurofilaments M and H that are present in a subset of pyramidal cells (Lee et al., 1987; Campbell and Morrison, 1989). PV preparations reveal a subset of GABAergic, nonpyramidal cells, such as basket and double bouquet interneurons (Celio, 1986; Condé et al., 1996; DeFelipe, 1997; Hof et al., 1999) that contain the calcium-binding PV protein. PV is also a useful marker that labels afferent cortical terminals from sensory thalamic nuclei (Van Brederode et al., 1990; DeFelipe and Jones, 1991; de Venecia et al., 1998; Hackett et al., 1998; Latawiec et al., 2000; Cruikshank et al., 2001; Wong and Kaas, 2008). CB, another calcium-binding protein, reveals a subset of GABA immunoreactive interneurons that are different from those revealed by PV (Van Brederode et al., 1990). VGluT2 immunostaining reveals thalamocortical terminations (Fujiyama et al., 2001; Kaneko and Fujiyama, 2002; Nahmani and Erisir, 2005; Wong and Kaas, 2008).

The use of several staining methods in this study allows us to provide more extensive descriptions of the architectonic subdivisions present in the neocortex of tree shrews. Comprehensive cortical maps with rigorous areal borders are more reliably established when the same borders are detected across different sections stained with different histological and immunohistochemical stains.

MATERIALS AND METHODS

The cortical architecture was studied in a total of eight adult *Tupaia belangeri*, which were kindly provided by David Fitzpatrick at Duke University. All experimental procedures were approved by the Vanderbilt Institutional Animal Care and Use Committee and followed the guidelines published by the National Institute of Health.

Tissue Preparation

The tree shrews were given a lethal dose of sodium pentobarbital (100 mg/kg). For visualizing synaptic zinc in the cortex, tree shrews were given 200 mg/kg body weight of sodium sulphide with 1 cc of heparin in 0.1 M phosphate buffer (PB) intravenously. Perfusion was carried out transcardially with phosphate-buffered saline (PBS), followed by 4% paraformaldehyde in 0.1 M PB, and 4% paraformaldehyde and 10% sucrose in PB. The brains were removed from the skull, bisected, and postfixed for 2–4 hr in 4% paraformaldehyde and 10% sucrose in PB. The hemispheres were placed in 30% sucrose overnight for cryoprotection before cutting on a freezing microtome into 40-μm-thick sections in the coronal, parasagittal, or horizontal planes. Brain sections were saved in four to five series. In some cases, the brains were artificially flattened, then cut tangentially at 40 μm, and saved in three series.

Histochemistry

One series of sections from each hemisphere was processed for Nissl substance (with thionin), and another series was processed for myelin, using the Gallyas (1979) silver procedure. In some cases, a third series of sections were processed for cytochrome oxidase (CO) (Wong-Riley, 1979).

Zinc Histochemistry

In tree shrews that were given intravenous injections of sodium sulfide, a series of sections was processed using the protocol outlined by Ichinohe et al. (2004) to visualize synaptic zinc. Brain sections were washed thoroughly with 0.1 M PB, followed by 0.01 M PB. The zinc-enriched terminals were visualized using the IntenSE M Silver enhancement kit (Amersham International, Little Chalfont Bucks, UK). The developing reagent was a one-to-one cocktail of the IntenSE M kit solution and 50% gum Arabic solution. The development of the sections was terminated, when a dark brown/black signal was seen, by rinsing sections in 0.01 M PB. Sections were then mounted and dehydrated in an ascending series of ethanols, (70% for 20 min, 95% for 10 min, 100% for 10 min), cleared in xylene, and coverslipped using Permount (Fisher Scientific, Pittsburgh, PA).

Immunohistochemistry

Each case contains one to two series of sections that have been immunostained for SMI-32 (1:2000; Covance, Princeton, NJ), parvalbumin (1:4000; Sigma-Aldrich, St. Louis, Mo), calbindin (CB) (1:5000; Swant, Bellinzona, Switzerland), or vesicle glutamate transporter 2 (1:4000; Chemicon now part of Millipore, Billerica, MA). Sections were incubated in their respective antibodies for 40–48 hr at 4°C. Details of the immunohistochemical procedures have been described in Wong and Kaas (2008).

Antibody Characterization

The anti-SMI-32 antibody is a mouse monoclonal antibody that specifically recognizes the 200-kD nonphosphorylated epitope in neurofilament H of most mammalian species. The epitope shows up as two bands (200 and 180 kDa) that merge into a single neurofilament H line on two-dimensional blots (manufacturer's technical information). The anti-SMI-32 antibody visualizes neuronal cell bodies, dendrites, and some thick axons in the nervous system and is not found in other cells and tissues. The mouse monoclonal anti-parvalbumin antibody specifically recognizes PV in a calcium ion-dependent manner and does not react with other members of the EF-hand family. On a two-dimensional gel, this anti-parvalbumin antibody specifically reacts with the Ca-binding spot of PV (MW = 12,000) from human, bovine, goat, pig, rabbit, canine, feline, rat, frog, and fish (manufacturer's technical information). The anti-calbindin antibody is a mouse monoclonal antibody produced by the hybridization of mouse myeloma cells with spleen cells from mice immunized with the calbindin D-28k that was purified from the chicken gut. It is not known to crossreact with other known calcium-binding proteins and specifically stains the 45 Ca-binding spot of calbindin D-28k (MW 28,000, IEP 4.8) from human, monkey, rabbit, rat, mouse, and chicken on a two-dimensional gel (manufacturer's technical information). The mouse monoclonal anti-VGluT2 antibody has shown species reactivity to the mouse and rat, and the antibody epitope for VGluT2 from Millipore is not known. However, preadsorption of this monoclonal antibody (MAB5504) with the C-terminal peptide (562–582) did not block staining (Wässle et al., 2006).

Light Microscopy

The architectonic borders were delineated from the brain sections that had undergone the various histochemical and immunohistochemical procedures described earlier. The locations of architectonic borders were determined by analysis of laminar and cell density changes in the processed sections when viewed at high power using a projection microscope. The Nissl, zinc, and VGluT2 preparations were most useful in identifying primary sensory areas, whereas sensorimotor cortical areas were better distinguished in the Nissl and SMI-32 preparations. Other histological preparations were used for corroborating ambiguous borders. Digital photomicrographs of sections were acquired using a Nikon DXM1200 (Nikon, Melville, NY) camera mounted on a Nikon E800 (Nikon, Melville, NY) microscope and adjusted for brightness and contrast using Adobe Photoshop (Adobe Systems, San Jose, CA).

Anatomical Reconstruction

Areal borders were reconstructed on surface views of the tree shrew brain as described in Wong and Kaas (2008). In brief, architectonic borders were identified and drawn for each outlined brain section using a

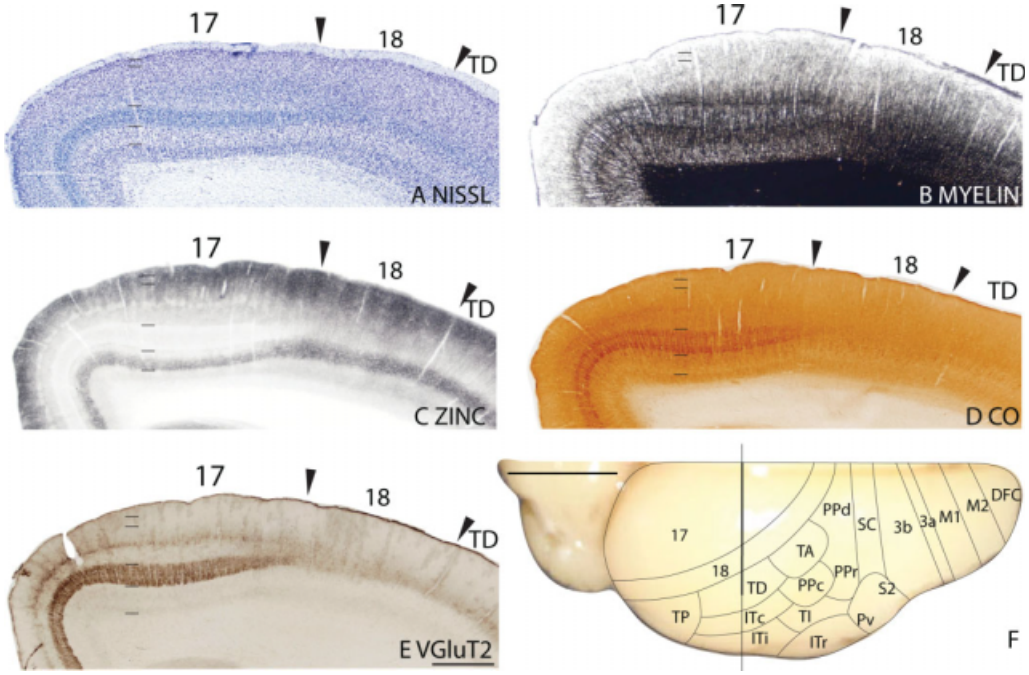

Fig. 1. Architectonic characteristics of visual areas 17, 18, and TD. Coronal sections from occipital cortex were processed for (**A**) Nissl substance, (**B**) myelin, (**C**) synaptic zinc, (**D**) CO, and (**E**) vesicle glutamate transporter 2 (VGluT2). The architectonic borders of proposed cortical areas are shown on the dorsal view of the tree shrew brain in panel **F**. The vertical line on the brain shows the level from which the sections were taken for panels A–E. The thicker portion of the line marks the regions illustrated in panels A–E. Occipital areas 17 and 18 are adopted from Brodmann (1909). TD is the temporal dorsal visual area. Arrowheads on the sections illustrated here and in the following figures mark architectonic boundaries. Short lines on the sections indicate cortical layers 1 to 6. See the abbreviations for other areas. The scale bar for brain sections (panel E) = 0.5 mm. The scale bar on the brain (panel F) = 5 mm.

Bausch and Lomb Microprojector (Bausch & Lomb, Rochester, NY). Adjacent brain sections were aligned based on blood vessels and other landmarks that were added to the section outlines. Outlines of brain sections with marked borders were imported into Adobe Illustrator (Adobe Systems, San Jose, CA) and aligned using the contour of the outline sections and the landmarks that were drawn. Brain surface views were reconstructed by projecting cortical and areal borders of selected brain sections onto lines appropriate for dorsal lateral, medial, and 45-degree angle view, and spacing these lines according to the location on the brain. Typically, the different histological procedures revealed similarly located boundaries between areas, suggesting that functionally relevant borders were being identified.

RESULTS

Our findings provide further evidence for several previously proposed subdivisions of neocortex in tree shrews (e.g., Zilles, 1978; Lyon et al., 1998; Remple et al., 2006), and evidence for areas that have not been previously described. Some of these proposed areas are shown on a dorsolateral view of the tree shrew brain in Fig. 1F. Descriptions of the cortical areas, by region, are as follows.

Occipital Cortex

The occipital region of tree shrews consists of areas 17 and 18, following Brodmann's (1909) terminology, and possibly areas lateral to area 18 that are included here in temporal cortex (Figs. 1–4). Areas 17 and 18 are architectonically distinct, and both fields are found to be coextensive with systematic retinal maps of the primary visual (V1) and secondary visual (V2) areas, respectively (Kaas et al., 1972). The visually responsive region lateral to area 18 has been divided into the temporal dorsal (TD), temporal anterior (TA), and temporal posterior (TP) regions (Kaas et al., 1972). Area TD lies in the middle portion along the rostral V2 border and shares some characteristics to the middle temporal visual area (MT) of primates, such as dense V1 input into the region, relative location, and dense myelination of area TD (Sesma et al., 1984; Kaas and Preuss, 1993; Lyon et al., 1998). Tracer injection studies have shown that area TP has connections with both V1 and V2 (Sesma et al., 1984; Lyon et al., 1998), and area TA has connections with V2 (Lyon et al., 1998).

Primary visual area, Area 17. Area 17 or striate cortex is a very architectonically distinct region with easily identifiable borders at low magnification (Fig. 1). The borders of area 17 are apparent even at low magnification in Nissl, fibers, zinc, CO, SMI-32, PV, and VGluT2 stains and are observed to be in similar locations (Figs. 1, 2). Area 17 is bordered rostrolaterally by extrastriate area 18 and extends medially onto the ventral surface of the hemisphere, where it is bordered by cortex known as the prostriata (PS) (Fig. 21). Laterally, layer 4 of area 17 tapers off near the 17/18 border (Figs.

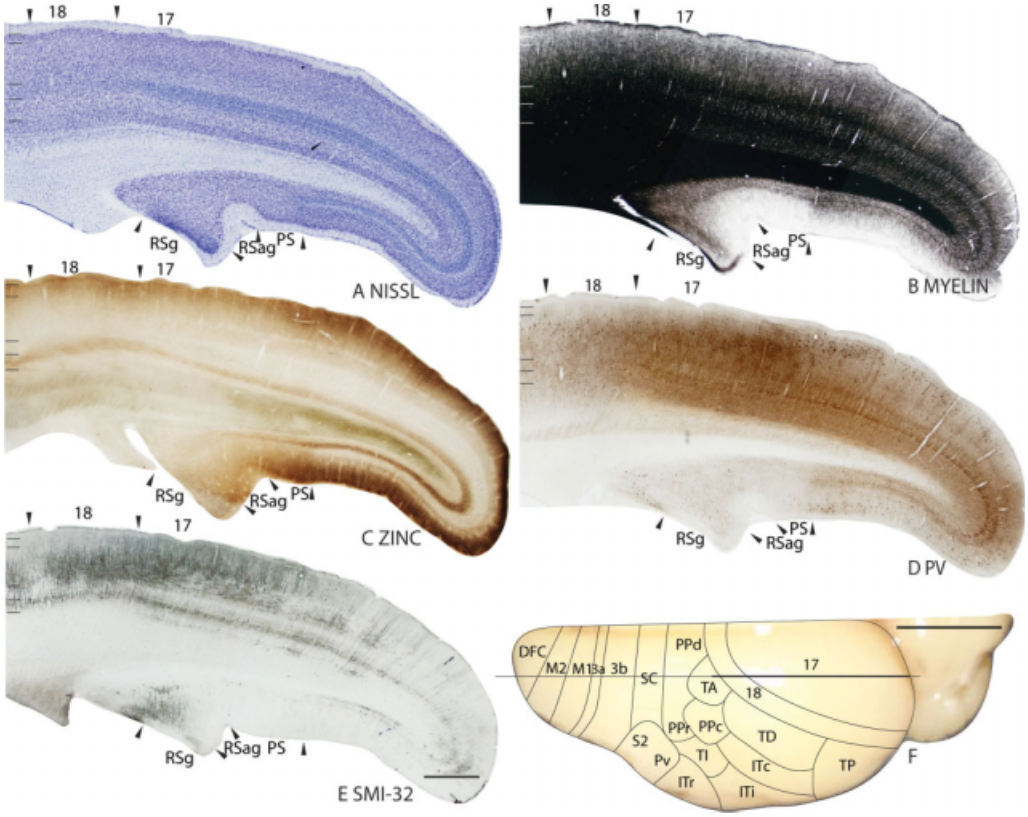

Fig. 2. Architectonic characteristics of visual areas and adjoining retrosplenial cortex. Parasagittal sections from occipital cortex were processed for (**A**) Nissl substance, (**B**) myelin, (**C**) synaptic zinc, (**D**) PV, and (**E**) neurofilaments with the SMI-32 antibody. The level at which the sagittal sections are taken from is indicated by the horizontal line on the dorsal view of the brain in panel **F**. The thicker line in panel F marks the regions illustrated in panels A–E. Short lines on the sections indicate the extent of each cortical layers 1 to 6. See the abbreviations for other areas. The scale bar for brain sections (panel E) = 1 mm. The scale bar on the brain (panel F) = 5 mm.

1, 2), where a transition zone of callosal connections with the other cerebral hemisphere may be located (Pritzel et al., 1988).

In Nissl preparations, layer 4 forms a dark band of densely populated granule cells (Figs. 1A, 2A). A cell-poor cleft in the middle of layer 4 is observed in sagittal sections, closer to the caudal portion of area 17 (Fig. 2A) (Conley et al., 1984; Jain et al., 1994). This cleft divides layer 4 into layers 4a and 4b, which receives projections from different layers of the geniculate nucleus (Harting et al., 1973; Conley et al., 1984). At higher magnifications (Fig. 3), area 17 has a layer 3 that is broad and divided into three sublayers, with layer 3a and 3c being less densely populated with cells than the middle layer 3b, and a layer 2 that has a dense population of small cells (Fig. 3A). The laminar features of area 17 can also be appreciated in sections processed for myelin, where the outer and inner band of Baillarger in layers 3c and 5, respectively, are revealed (Figs. 1B, 2B, 3B). Note that the outer band of Baillarger, also known as the stria of Gennari, is coextensive with layer 3C in Nissl stains and is not in layer 4 as commonly depicted for primates. The two bands of Baillarger are not apparent laterally in area 18, and medially in PS, which is poorly myelinated, allowing the delimitation of the area 17/18 and 17/PS areal borders.

In CO preparations, layer 4 is darkly stained (Figs. 1D, 3C), whereas middle layer 3 is lightly stained (Fig. 1D). Layer 4 is darkly stained for PV in area 17 (Figs. 2E, 3G) and tapers off at the 17/18 border (Fig. 2E). Layers 3a and 3b showed darkly stained cell bodies immunoreactive for PV (Fig. 3G). SMI-32 staining of area 17 is not homogenous, with more pyramidal cells labeled closer to the rostral border of area 17 (Fig. 2E). At higher magnifications, the SMI-32 stain revealed dark bands of pyramidal neurons in layers 3 and 5, with some staining in inner layer 6, and no SMI-32 immunopositive cell bodies in layer 4 (Fig. 3D). Layers 1, 2, and 3a of area 17 express high levels of CB, with a dense population of CB-immunoreactive cell bodies (Fig. 3H).

Layer 4 of area 17 expresses very little synaptic zinc, standing out as a white band (Figs. 1C, 2C, 3E), and layers 1 to 3b and 5b stain darker than the rest of the cortical layers in area 17 (Fig. 3E). The adjacent area 18 and PS express more synaptic zinc in layer 4 (Figs. 1C, 2C). Layers 3, especially inner layer 3, and 6 show higher levels of zinc stain than layer 4, but lower levels than the corresponding layers of the adjacent cortices. The lower levels of zinc staining in layers 3 and 6 suggest that there are a greater proportion of thalamic terminations in these layers than in adjoining areas of cortex. The lateral geniculate nucleus of tree shrews has

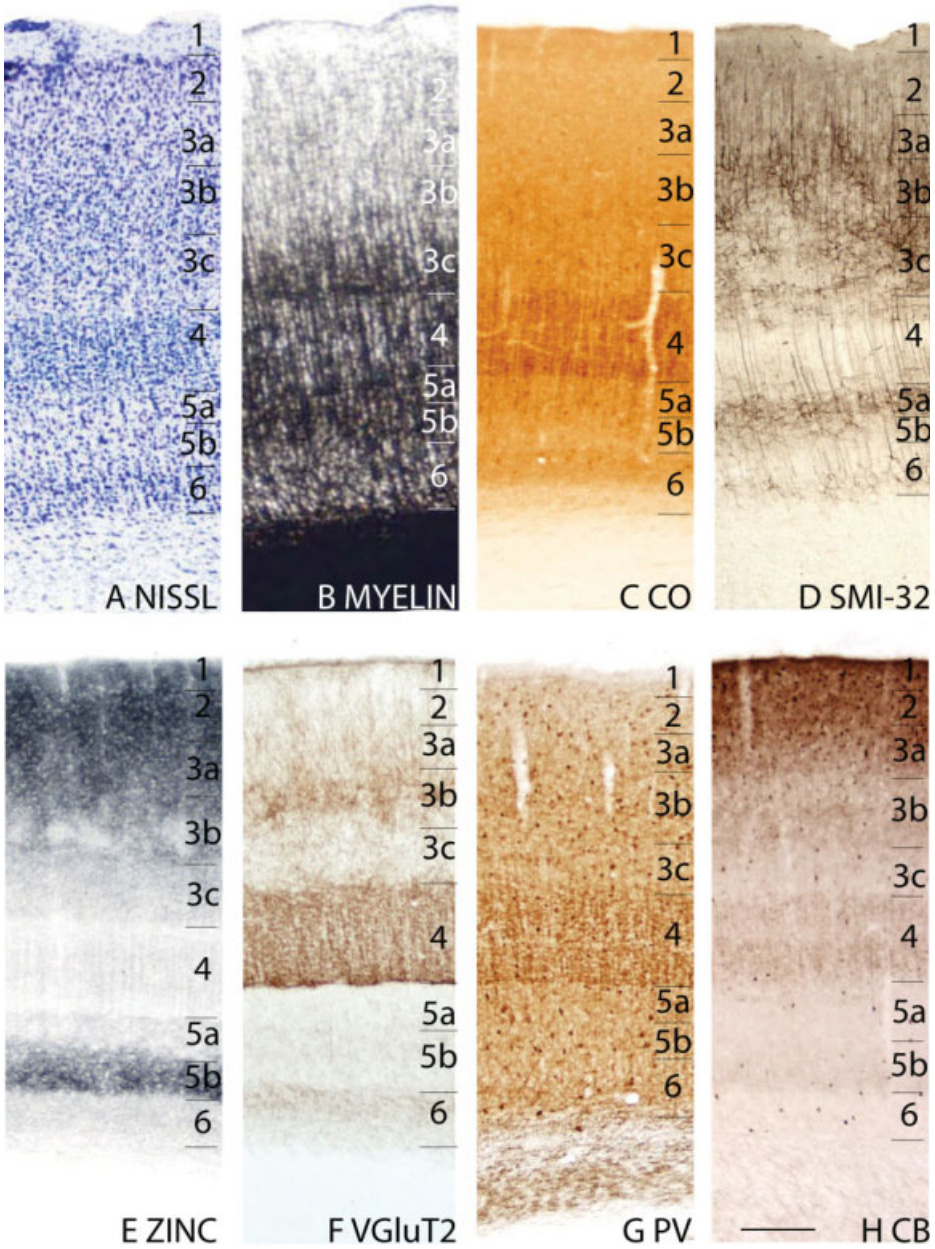

Fig. 3. The laminar characteristics of area 17 at higher magnification. The sublayers of layer 3 are apparent in the Nissl, synaptic zinc, VGluT2, and CB preparations. Layer 5 has two sublayers, 5a and 5b, that are apparent in Nissl, CO, SMI-32, and zinc preparations. Scale bar = 0.25 mm.

major projections to layer 4 and minor projections to layers 3b, 3c, and 6 (Conley et al., 1984). In coronal sections and at higher magnification, the zinc stain also reveals a patchy pattern in layer 3b (Figs. 1C, 3E).

In artificially flattened cortex, a pattern of myelin-poor patches surrounded by myelin-rich regions is observed in layer 3 (Figs. 4A,B). In addition, there are circular regions, resembling "walls," darkly stained for zinc, surrounding zinc-poor centers (Fig. 4D). In VGluT2-stained sections, layer 4 is darkly stained in area 17 compared with the adjoining cortical areas (Fig. 1E). Small, dark patches of VGluT2 staining seem to correspond to the zinc-poor centers in layer 3c (Fig. 3F). The patchy staining pattern is observed in sections of flattened cortex through layer 3 (Fig. 4C). This suggests that thalamocortical and corticocortical projections follow some form of modular organization in layer 3b of the tree shrew's primary visual cortex, whereby thalamic projections are clustered in patches surrounded by "walls" of corticocortical projections. This is reminiscent of the projections of the koniocellular layers of the lateral geniculate layer to layer 3 of area 17 in primates

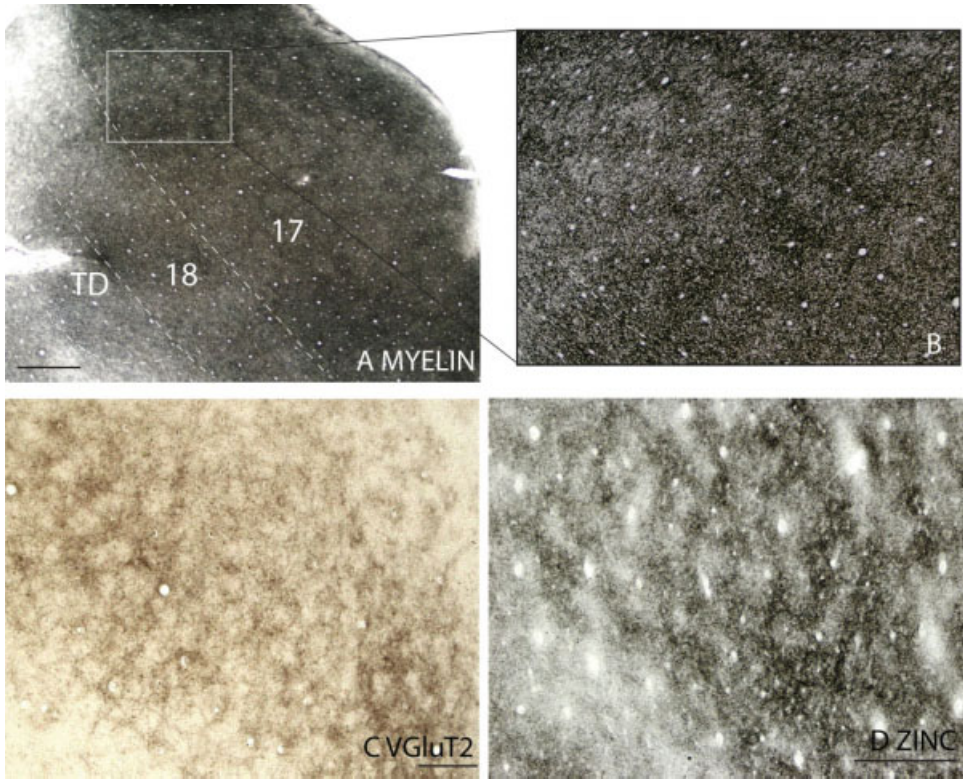

Fig. 4. Patchy staining pattern of area 17. (**A**) A myelin-stained section cut parallel to the surface of an artificially flattened cerebral hemisphere. Dashed lines show the approximate location of the cortical borders. The boxed region in A is shown in **B** at higher magnification. **C** and **D** are from a different case and show the patchy staining pattern of area 17 in VGluT2 and zinc preparations. Scale bar in panel A = 0.5 mm, for panel B and C = 0.5 mm, for panel D = 250 μm.

(e.g., Weber et al., 1983; see Casagrande and Kaas, 1994, for review), and the "honeycomb" structure that has been described in the layers 1 and 2 of visual cortex in rats (Ichinohe et al., 2003). It is also interesting to note that the VGluT2-rich patches and zinc-poor patches are smaller in size compared with the myelin-poor patches (Fig. 4).

Second visual area, Area 18. Area 18 in the tree shrews lies along the lateral border of the primary visual area, V1 or area 17, and is approximately one-third the size of area 17 (Sesma et al., 1984). Electrophysiological recordings revealed that area 18 is coextensive with the second visual area, V2, and contains a representation of the contralateral visual hemifield that is an approximate mirror reversal of that in area 17 (Kaas et al., 1972).

The laminar pattern of area 18 is less distinct than area 17. As shown in Nissl preparations (Figs. 1A, 2A), layers 4 and 6 in area 18 are less densely packed with granular cells compared with area 17. Layer 5 is more sparsely populated with cells than the three cortical areas TA, TD, and TP that lie lateral to V2 (Figs. 6A, 8A). In sections stained for myelin, the distinct outer and inner bands of Baillarger that are present in area 17 are absent in area 18, although area 18 has a moderately high level of myelination (Figs. 1B, 2B) that is higher than the cortical areas along its lateral border (Figs. 4B, 6B). In sections stained for zinc, area 18 shows increased staining in layer 4, suggesting less thalamic and more corticocortical inputs are present. Layer 5 is thicker and more darkly stained compared with area 17 (Fig. 1C). The intensity of zinc staining in layer 4 of area 18 is higher than in area TD (Figs. 1C, 7C, 8C), but is lower than in areas TA and TP (Fig. 6C, not shown). As such, area TD likely receives proportionally more thalamic inputs than areas 18, TA and TP, whereas area TA and TP receives proportionately the most cortical inputs. Layer 4 of area 18 shows lower levels of CO staining compared with area 17 (Fig. 1D).

Layers 4 and 6 express less PV (Fig. 2D) and VGluT2 (Fig. 1E) in area 18 than area 17. In SMI-32 preparations, area 18 shows a higher density of pyramidal cells in layer 3 compared with area 17 (Fig. 2E). Additionally, the SMI-32-immunoreactive pyramidal cells in 5 of area 18 are larger and have shorter apical dendrites than those in area 17 (Fig. 2E).

Temporal Visual Cortex

Originally identified as area 19 by Kaas et al. (1972), the strip of cortex lateral to area 18 has since been divided into three architectonically distinct areas, TA, TD, and TP (Sesma et al., 1984; Lyon et al., 1998). These three areas receive projections from area 17, with TD receiving the densest inputs, followed by TP, then TA

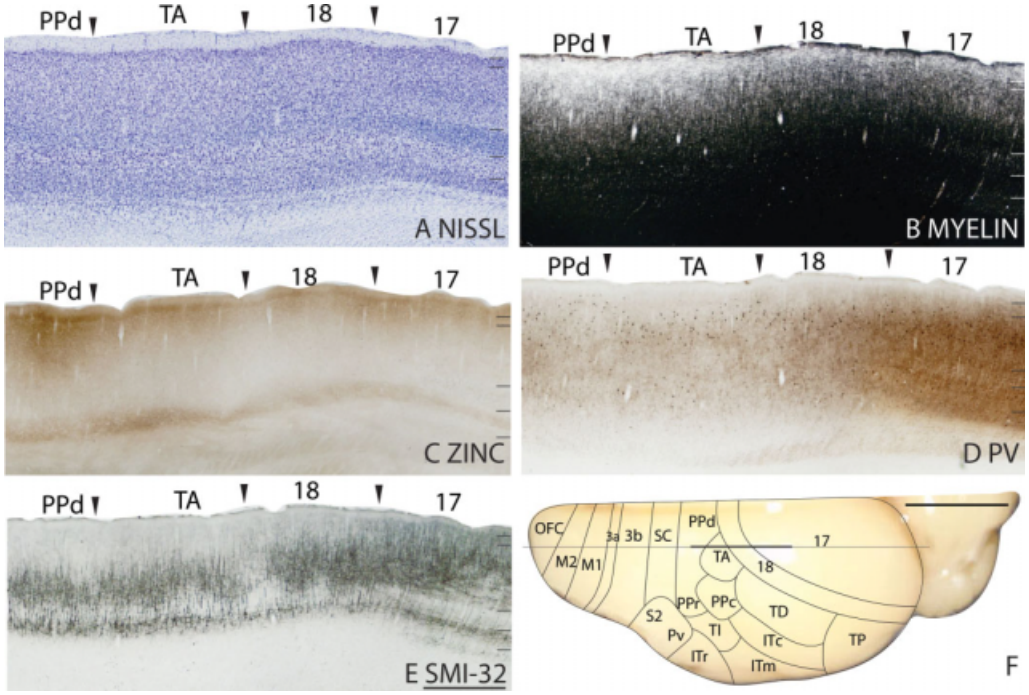

Fig. 5. Architectonic characteristics of visual and temporal visual areas. The level at which the sagittal sections are taken from is indicated by the horizontal line on the dorsal view of the brain in panel **F**. The thicker line in panel F marks the regions illustrated in panels **A**–**E**. The extent of each cortical layers 1 to 6 is indicated by the short horizontal lines on panels A–E. The scale bar for brain sections (panel E) = 1 mm. The scale bar on the brain (panel F) = 5 mm.

with the fewest inputs (Sesma et al., 1984; Lyon et al., 1998). In sections processed for the Cat-301 antibody, both TD and TA expressed more of the antigen for Cat-301 than TP (Jain et al., 1994).

Temporal anterior area. In the Nissl stain, area TA has a thinner layer 4 and a more densely packed layer 5 with larger pyramidal cells than area 18 (Fig. 5A). Area TA is less well myelinated than both area 18 and TD. There are higher levels of synaptic zinc in TA, with a thicker, more darkly stained layer 5 compared with area 18 (Fig. 5C). In CO preparations, layer 4 is somewhat darker stained in area TA than in area 18, but is lighter stained than in the ventrally located posterior parietal caudal area (PPc) (not shown).

Layer 4 of area TA has much lower immunoreactivity levels for both PV (Fig. 5D) and VGluT2 than the adjoining areas (not shown). SMI-32 immunostaining reveals darkly stained pyramidal cells in layers 3 and 5 of area TA with layer 5 being more densely packed with pyramidal cells than the adjoining area 18 (Fig. 5E). The pyramidal cells in layer 3 have shorter apical dendrites compared with those in area 18. The distribution of SMI-32-immunopositive pyramidal cells in layers 3 and 5 of TA is similar to that of PPd (Fig. 5E).

Temporal dorsal area. Area TD is about 6 mm long and 2 to 3 mm wide (Sesma et al., 1984). Based on its relative location, connection pattern with area 17, myeloarchitecture, and Cat-301 immunostaining characteristics, area TD has been proposed as a possible homologue of the primate MT (Sesma at al., 1984; Kaas and Preuss, 1993; Jain et al., 1994; Northcutt and Kaas, 1995).

Near the area 18/TD border, sections processed for Nissl bodies reveal a reasonably well-developed layer 4 in area TD that is thicker than in area 18 (Figs. 1A, 7A), but much less populated with granule cells than in area 17 (Figs. 1A, 7A). Layer 5 of area TD was packed with pyramidal cells that were larger than those in area 18 (Fig. 1A), but smaller than those in the inferior temporal caudal area (ITc). The distribution densities of cells do not seem to be homogeneous in area TD. Away from the 18/TD border, the density of cells in layer 4 increases (Fig. 7A). Area TD is slightly more myelinated than area TA (not shown), TP (Fig. 7B), and ITc (Fig. 6B) but is less myelinated than area 18 (Figs. 1B, 7B). As observed in the Nissl stain, the myelination level of area TD is not uniform and increases gradually away from the 18/TD border (Fig. 7B). In the zinc stain, layers 3 and 5 of area TD are more intensely stained compared with area 18 (Figs. 1C, 8A) and are similarly stained to that of TP (Fig. 8A). The distribution of free ionic zinc in layer 4 of area TD is lower than in areas 18 and TP (Fig. 8A). In flattened cortex, layer 4 of area TD has higher levels of CO activity than area 18 and similar levels to ITc (Fig. 6C).

In PV preparations, two bands of PV-immunopositive terminations, reflecting thalamic inputs, are observed, one dark band in layer 4 and a lighter band in layer 6. Layers 4 and 6 of area TD are more immunoreactive for PV than either area 18 or TP. The immunoreactivity of layer 4 for PV increases away from the 18/TD border (Fig. 7C). TD stains poorly for VGluT2, with layer 4

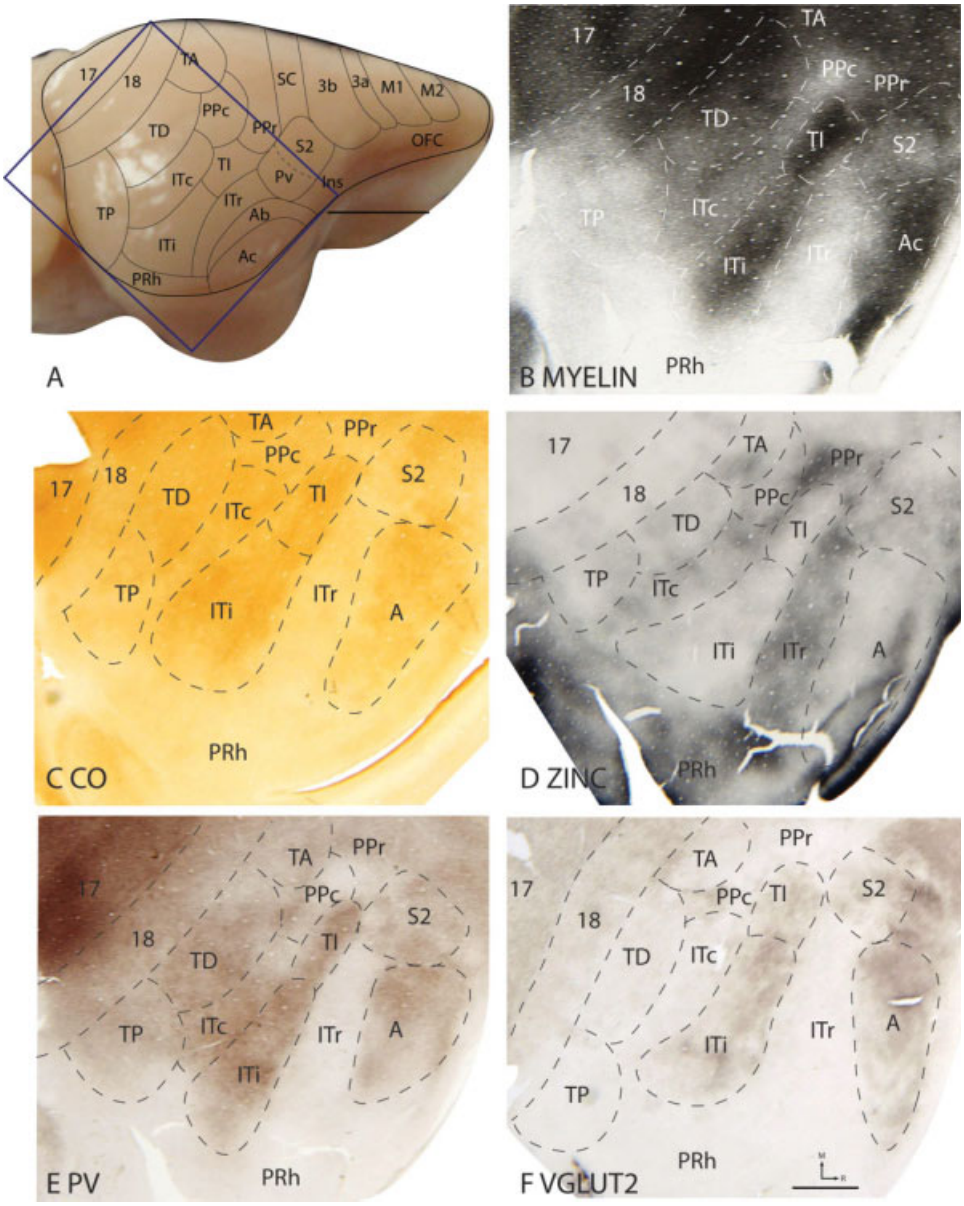

Fig. 6. Architectonic characteristics of temporal and inferior temporal cortex in flattened preparations. (**A**) Architectonic borders of proposed cortical areas are shown on the lateral view of the tree shrew brain. The box indicates the regions that are illustrated in panels **B–F**. Sections in panels B to F are cut parallel to the surface of an artificially flattened cerebral hemisphere and show the topographic organization of the areas in the temporal and inferior temporal cortex. Scale bar in panel A = 5 mm, in panel F = 2 mm.

being less intensely stained for VGluT2 than in area 18 (Figs. 1E, 6F). There is no noticeable difference between the levels of VGluT2 staining in TD and TP (Fig. 6F). SMI-32 staining in TD is less than in ITc (Fig. 10K), but is darker than in TP (not shown). The pyramidal cells in layers 3 and 5 of area TD stain darker for the SMI-32 antibody compared with area 18; however, they have shorter apical dendrites (Fig. 8C). As the staining pattern gradually changes somewhat from medial to lateral, it is possible that TD represents the visual field from central to peripheral vision.

Temporal posterior area. Area TP covers an area of ~10 mm^2 (Sesma et al., 1984), and as revealed by the Nissl stain, is less densely populated with cells in layers 2 and 3 than the adjoining area 18 (Fig. 7A). Layer 4 of TP is more densely populated by granule cells than the adjoining ITi (Fig. 9B). TP is less myelinated than both area 18 and TD (Fig. 7B). The myelination levels of TP and ITi are similar (Fig. 9C). The TP/PRh border is distinctly marked by the lack of myelination in PRh (Fig. 9C). In CO preparations, layer 4 of area TP stains

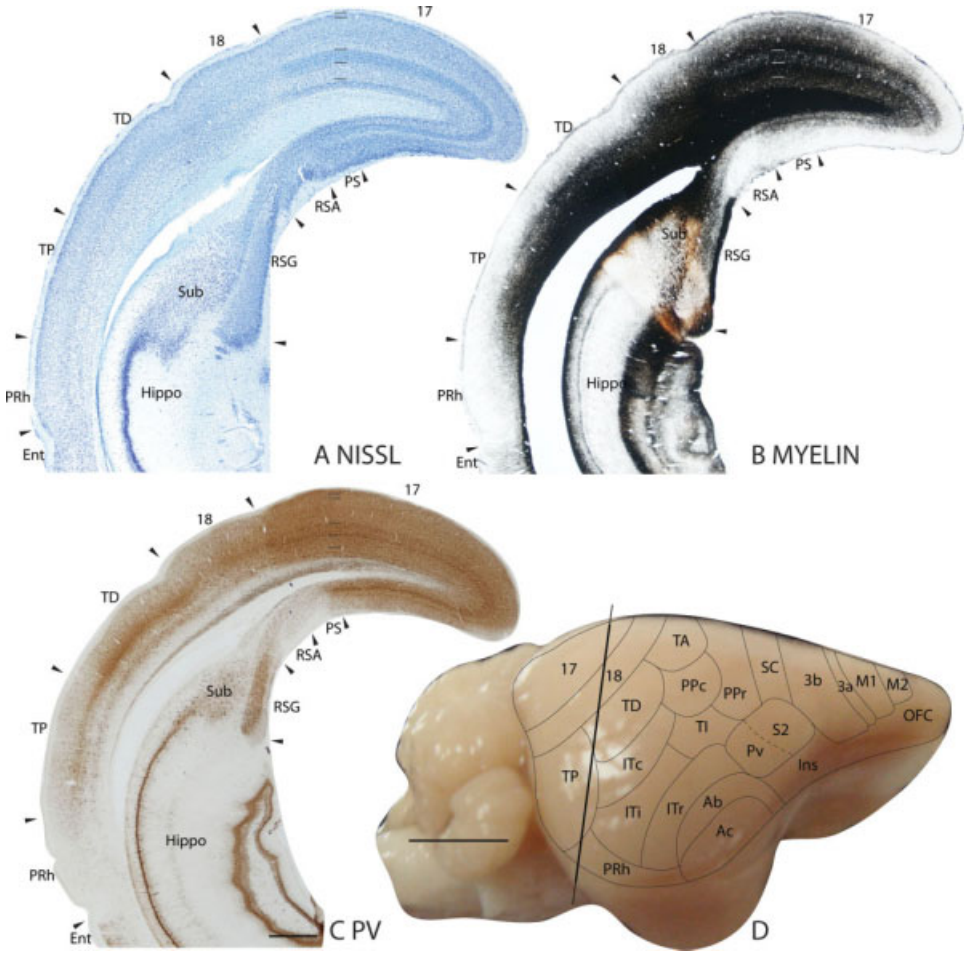

Fig. 7. Architectonic characteristics of occipital and temporal visual areas. The location from which the coronal sections are taken from is indicated by the vertical line on the lateral view of the brain in panel **D**. The thicker portion of the line indicates the region that is illustrated in panels **A–C**. The scale bar for brain sections (panel C) = 1 mm. The scale bar on the brain (panel D) = 5 mm.

darker than layer 4 of area 18 (not shown), and is lighter stained than layer 4 of ITi (Fig. 9C) and ITc (not shown). There is an overall increase in the intensity of zinc staining across the cortical layers of area TP compared with the adjoining area 18, TD (Fig. 7E), ITi (Fig. 9E), and ITc (not shown). However, the level of zinc staining in TP is still lower than that of PRh (Figs. 7E, 9E).

In PV preparations, there is one thin but distinct band of PV-immunopositive terminations in layer 4 of TP, and a faint band in layer 6. TP is lightly stained for the PV antibody compared with TD, but more darkly stained than PRh (Fig. 7C). TP stains poorly for both SMI-32 and VGluT2 (not shown).

Temporal inferior area. Ti has a well-developed layer 4 that is densely populated with cells in Nissl-stained sections (Figs. 10G, 11A). Layer 5 of TI is more densely populated with cells than ITr (Figs. 10G, 11A) and ITc (Fig. 10G), and has smaller cells compared with PPc (Fig. 11A). In the myelin stain, TI is more densely myelinated than the surrounding areas (Figs. 6B, 10H, 11B), with a band of myelinated fibers in inner layer 3 (Fig. 10H). In flattened cortex stained for CO, TI is a darkly stained oval (Fig. 6C). In coronal sections, two bands of CO staining, in layers 4 and 6, are present in TI, and absent in PPc and ITr (Fig. 11D). Layer 4 of TI stains poorly for the zinc stain, as such, the borders of TI with the surrounding cortical areas are distinct in the zinc stain (Figs. 6D, 10I, 11C).

TI stains darkly for PV with a band of PV-immunopositive terminations in layer 4, and also note the scattering of PV-positive cells (Fig. 10J). In flattened cortex, TI is a darkly stained oval in PV preparations (Fig. 6E). TI also stains darkly for VGluT2 compared with the surrounding areas in flattened cortex (Fig. 6F), and in coronal sections, has a dense band in layer 4, and a lighter band in layer 6 (Fig. 11E). In SMI-32 preparations, layer 5 of TI has darkly stained SMI-32-immunopositive pyramidal neurons (Fig. 10J).

Inferior Temporal Cortex

The organization of inferior temporal (IT) cortex in tree shrews has not been extensively studied. Zilles (1978) considered IT cortex of tree shrews to be as a

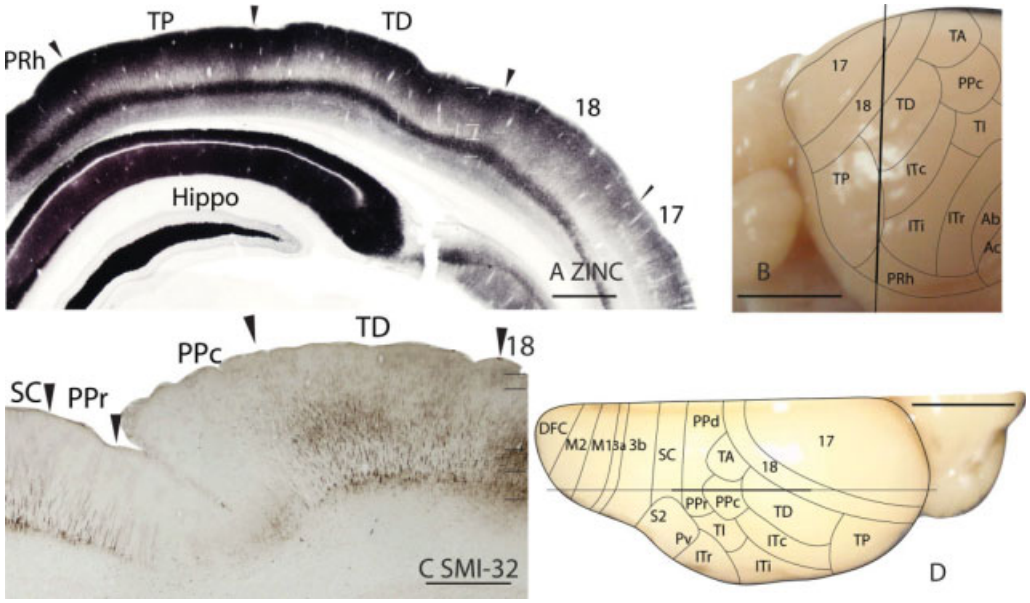

Fig. 8. Architectonic characteristics of the temporal dorsal area. (**A**) A coronal section stained for synaptic zinc. The level at which this section is taken from is indicated by the vertical line on the lateral view of the tree shrew brain. (**C**) A parasagittal section stained for the SMI-32 antibody to reveal neurofilaments. The horizontal line on the dorsal view of the tree shrew brain in **D** indicates the location from which the section in panel C is taken from. The scale bar for brain sections (panels A and C) = 1 mm. The scale bar on the brain (panels **B** and D) = 5 mm.

single area, area temporalis 3 (Te3). More recently, Remple et al. (2007) divided IT cortex into at least three areas, the temporal inferior area (TI), the temporal posterior inferior area (TPI), and, the rest of IT cortex surrounding these two areas, the temporal inferior ventral (TIV) area. In this study, IT cortex has been divided into four areas, inferior temporal rostral (ITr), inferior temporal intermediate (ITi), ITc, and TI. ITi is similar to TPI of the Remple et al.'s (2007) study.

Inferior temporal rostral area. In Nissl preparations, layer 4 of ITr is less densely packed with granule cells than layer 4 of auditory cortex (Fig. 9B), TI (Fig. 11A), and ITi (Fig. 10A). However, layer 4 of ITr is more distinct than layer 4 of PRh (Fig. 10A). ITr is less myelinated (Figs. 9C, 10B, 11B) than the cortical areas surrounding it, except for PRh (Figs. 9D, 10C, 11C), and this is observed in artificially flattened cortex as well (Fig. 6B). ITr expresses more free ionic zinc, especially in layer 4, compared with the auditory cortex (Fig. 9E), TI (Fig. 11C), and ITi (Figs. 9D, 10C). Compared with PRh, ITr expresses less free ionic zinc across all the cortical layers, with the greatest difference in layer 4 (Fig. 10C). At higher magnification, CO staining is observed in layer 5 of ITr, but very little CO staining is present in layers 4 and 6 (Fig. 11C). ITr expresses less CO protein than the surrounding cortical areas (Fig. 6C), such as Ti (Fig. 11D), auditory cortex (Fig. 9D), and ITi (Figs. 9D, 10D), and is more darkly stained for CO than PRh (Figs. 9D, 10D).

ITr stains poorly for PV (Fig. 6E) and VGluT2 (Fig. 6F) compared with the surrounding cortical areas. Sections stained for SMI-32 revealed a sparse population of pyramidal cells in layer 5 (Fig. 10K).

Inferior temporal intermediate area. In Nissl preparations, ITi has a thicker and more densely packed layer 4 than ITr, and a thicker, but less densely packed layer 4 than ITc (Fig. 10A). Layer 5 of ITi is sparsely populated, and the size of cells is smaller compared with both ITc and ITr (Fig. 10A). Layer 4 of ITi is thicker but more sparsely populated than the adjoining TP, and layer 5 is thinner and populated with smaller cells than in TP (Fig. 9B). In myelin preparations, ITi is more myelinated than the bordering areas, ITc and ITr (Fig. 10B), and has a similar level of myelination compared with TP (Fig. 9C). In flattened cortex, ITi stands out as a darkly myelinated oval (Fig. 6B). ITi expresses more CO protein than both ITr and TP (Figs. 9D, 10D), and expresses a similar level of CO to ITc (Fig. 10D). In flattened cortex, ITi is an oval region that stains darker for CO than the surrounding regions (Fig. 6C). ITi expresses less free ionic zinc than ITr across all the cortical layers, and this is most obvious in layer 4 (Figs. 9D, 10C). The zinc staining in ITi is slightly lower than that in both TP (Fig. 9E) and ITc (Fig. 10C). In flattened cortical sections stained for zinc, ITi is a light patch surrounded by darker stained areas (Fig. 6D).

ITi stains darker for PV than ITr and TP, and to a lesser extent, ITc as well (Fig. 6E). In VGluT2 preparations, layer 4 of ITi is thicker and darker stained than TP (Fig. 6F), ITc, and ITr (Fig. 10E). ITi stains poorly with the SMI-32 antibody (not shown).

Inferior temporal caudal area. In Nissl preparations, ITc has a thinner layer 4 compared with ITi (Fig. 10A) and TD (Fig. 10G), and a less densely populated layer 4 than in TI (Fig. 10G). Layer 5 of ITc is less populated with cells than TI (Fig. 10G), and more populated with cells than ITi (Fig. 10A) and TD (Fig. 10G). ITc has

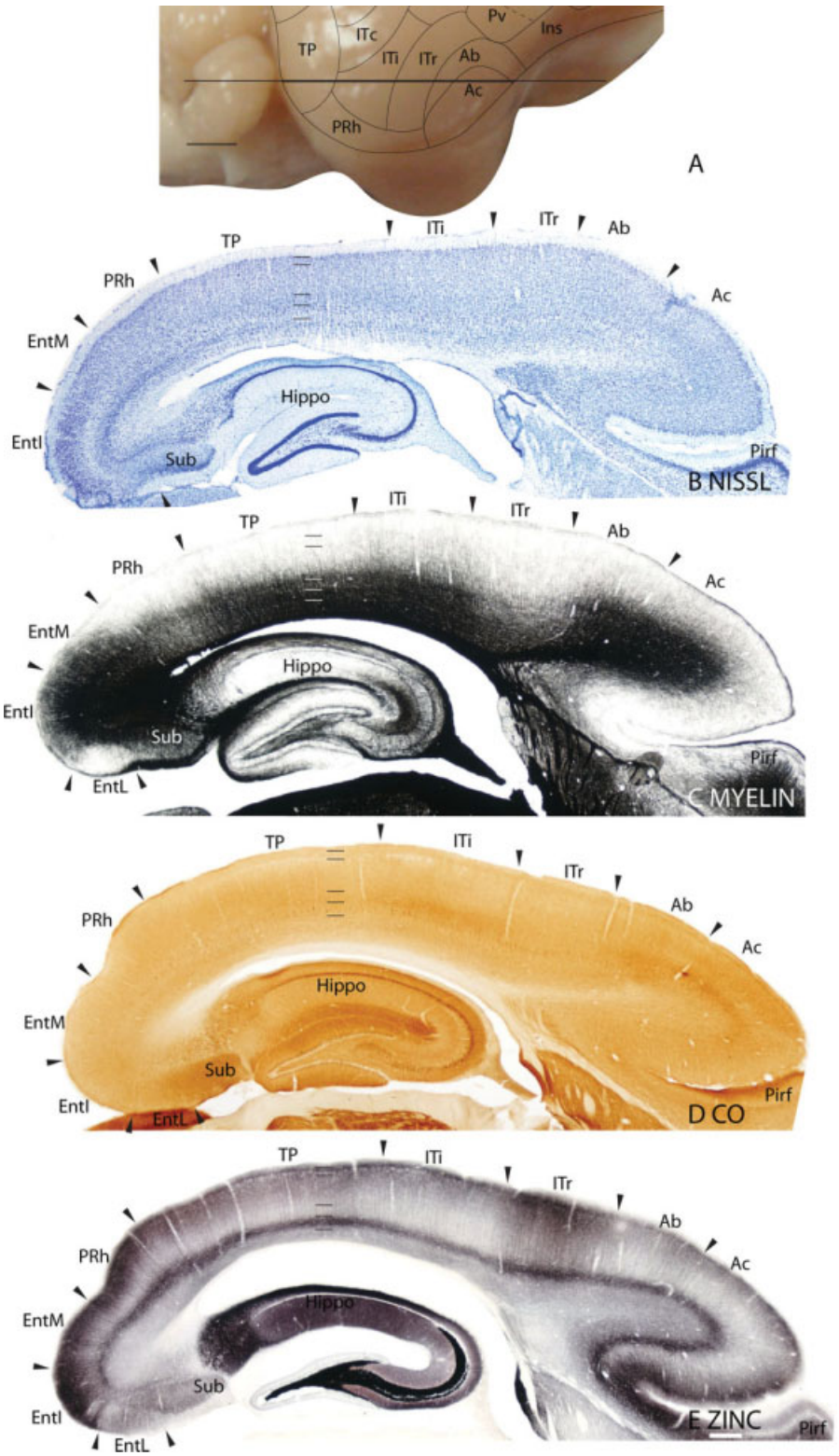

Fig. 9. Architectonic characteristics of the temporal posterior and inferior temporal areas. Cortical areas are shown on a lateral view of the ventral hemisphere in panel **A**. The thicker portion of the horizontal line across the brain indicates the location of the horizontal brain sections illustrated in panels **B**–**E**. The scale bar for brain sections (panel E) = 0.5 mm. The scale bar on the brain (panel F) = 5 mm.

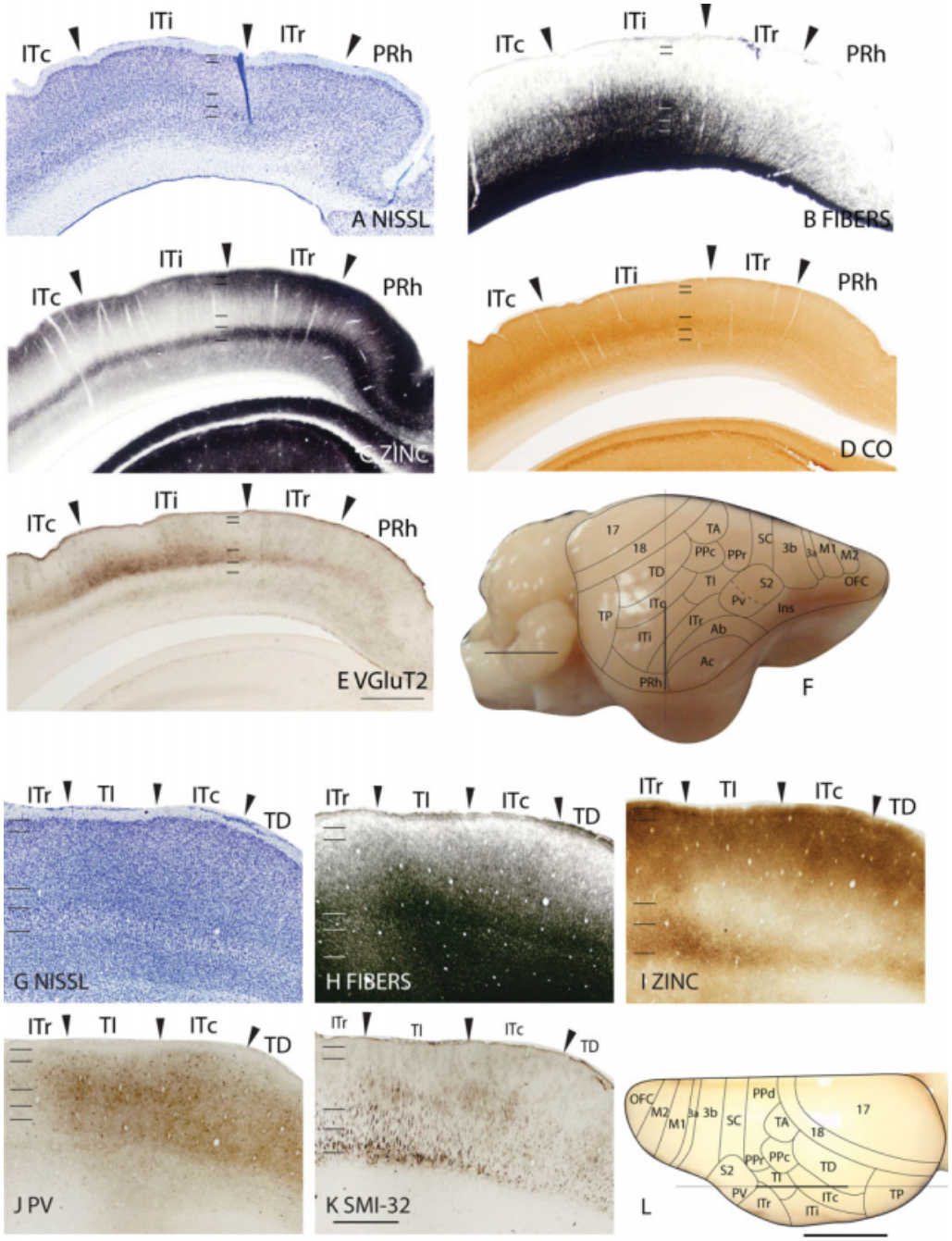

Fig. 10. Architectonic characteristics of the inferior temporal areas. Panels **A–E** are coronal sections taken from the approximate location indicated by the vertical line on the lateral view of the tree shrew brain in panel **F**. Panels **G–K** are parasagittal sections take from the approximate location indicated by the horizontal line on the dorsal view of the tree shrew brain in panel **L**. The scale bar for brain sections (panels E and K) = 1 mm. The scale bar on the brain (panels F and L) = 5 mm.

lower levels of myelination compared with the surrounding areas TD, TI, and ITi (Figs. 6B, 10B, 10H). ITc expresses similar levels of CO to TD (Fig. 6C), and less CO than TI and ITi (Figs. 6C, 10D). In the zinc stain, ITc expresses more free zinc ions than TI (Figs. 6D, 10I) and ITi (Figs. 6D, 10C), especially in the upper cortical layers. ITc expresses less free zinc ions, especially in layer 4, than TD (Figs. 6D, 10I).

In PV preparations, more labeled cells are observed in layers 2 and 3 than in layers 4, 5, and 6 (Fig. 10J). ITc stains less intensely for PV-immunopositive terminals than both ITi and TI (Figs. 6E, 10J). Layer 4 of ITc stains less intensely for VGluT2 than in layer 4 of ITi (Figs. 6F, 10E) and TI (Fig. 6F). In SMI-32-immunostained sections, ITc has a sparser distribution of SMI-32-labeled pyramidal cells compared with TI (Fig. 10K).

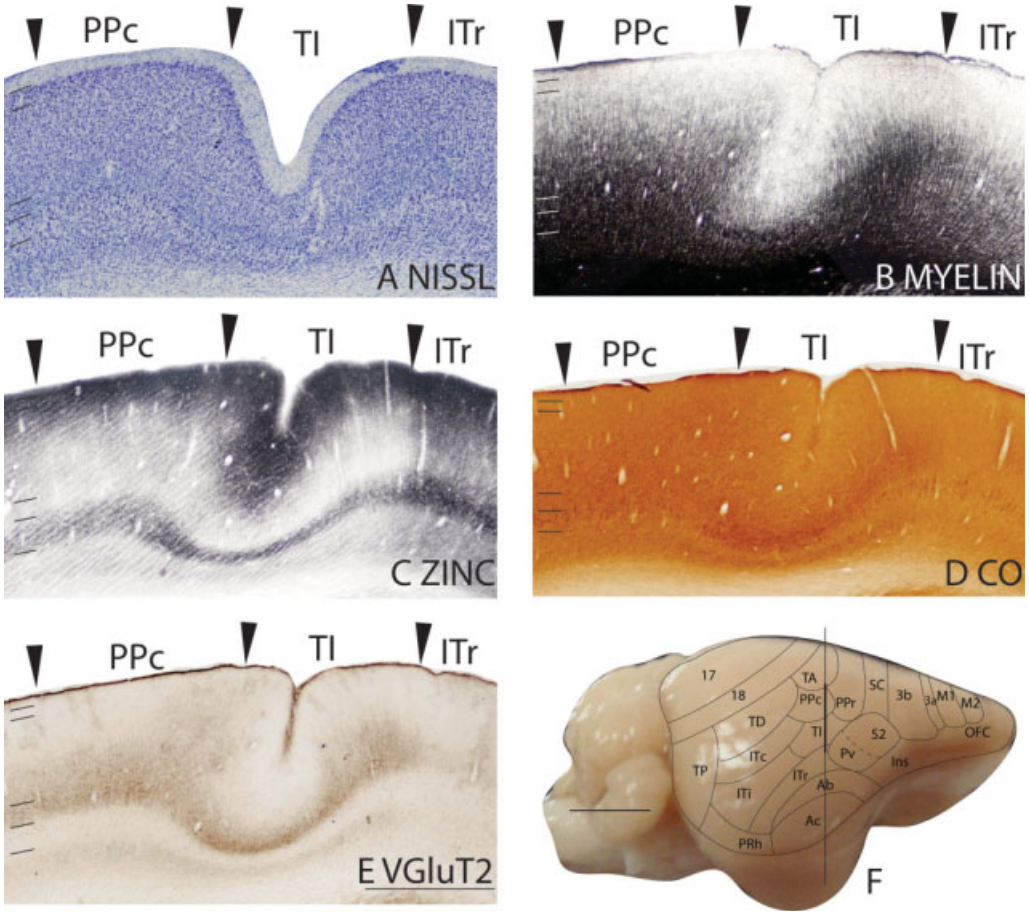

Fig. 11. Architectonic characteristics of the temporal intermediate area and adjoining areas. Cortical areas are shown on a lateral view of the right hemisphere in panel **F**. The thicker part of the vertical line across the brain indicates the location of the coronal brain sections illustrated in panels **A–E**. The scale bar for brain sections (panel E) = 1 mm. The scale bar on the brain (panel F) = 5 mm.

Auditory Cortex

The auditory cortex of tree shrews contains a primary auditory core (Ac) of one or more primary auditory areas (Diamond et al., 1970; Oliver and Hall, 1975, 1978; Casseday et al., 1976) and a bordering auditory belt (Ab), which wraps around the mediorostral border of the primary Ac (Oliver and Hall, 1978). Ac extends ventrally into the rhinal fissure, where it abuts the ectorhinal cortex (Ect).

Primary auditory core. The primary Ac is characterized by a thick layer 4 that is densely populated by small granule cells in the Nissl stain, and by a layer 5 that contains medium-sized pyramidal cells in the outer sublayer of layer 5 (Fig. 12A). Ac is well myelinated, with distinct outer and inner bands of Baillarger that are absent in Ect (Fig. 12B). In CO preparations, layer 4 of Ac stains darker than the surrounding areas, Ab and Ect (Fig. 12D). Layer 4 of Ac stains poorly for free zinc ions, and as such shows up as a white band, providing a sharp ventral border with Ect (Fig. 12C).

In VGluT2 preparations, layer 4 of Ac is a wide band that is more intensely stained compared with the surrounding areas, Ab and Ect (Fig. 12E). Neurons stained for PV are present throughout the cortical layers in Ac (Fig. 13A). Layer 4 of Ac stains darkly for PV-immunopositive terminations, and this staining terminates at the Ac/Ect border (Fig. 13A). Small SMI-32-immunopositive pyramidal neurons densely populate layer 3, and a few SMI-32-stained pyramidal cells are observed in layer 5 of Ac (Fig. 13B).

Auditory belt. Ab has a thinner layer 4 than Ac, but is thicker than in Pv (Fig. 12A). In the Nissl stain, the granule cells in layer 4 of Ab are larger and more darkly stained than those in Ac, and in layer 3, the cells are larger in Ab than in Ac (Fig. 12A). Ab is more heavily myelinated than Pv and has similar myelination levels to Ac (Fig. 12B). Like Ac, Ab expresses low levels of free zinc ions in layer 4; as such, layer 4 of Ab is a white band in zinc-stained sections (Fig. 12C). Layer 4 of Ab stains more darkly for CO than in Pv and is more lightly stained and thinner than in Ac (Fig. 12D).

In VGluT2 preparations, layer 4 of Ab stains darkly for VGluT2-immunopositive terminations compared with the adjoining Pv, and is thinner and less intense in

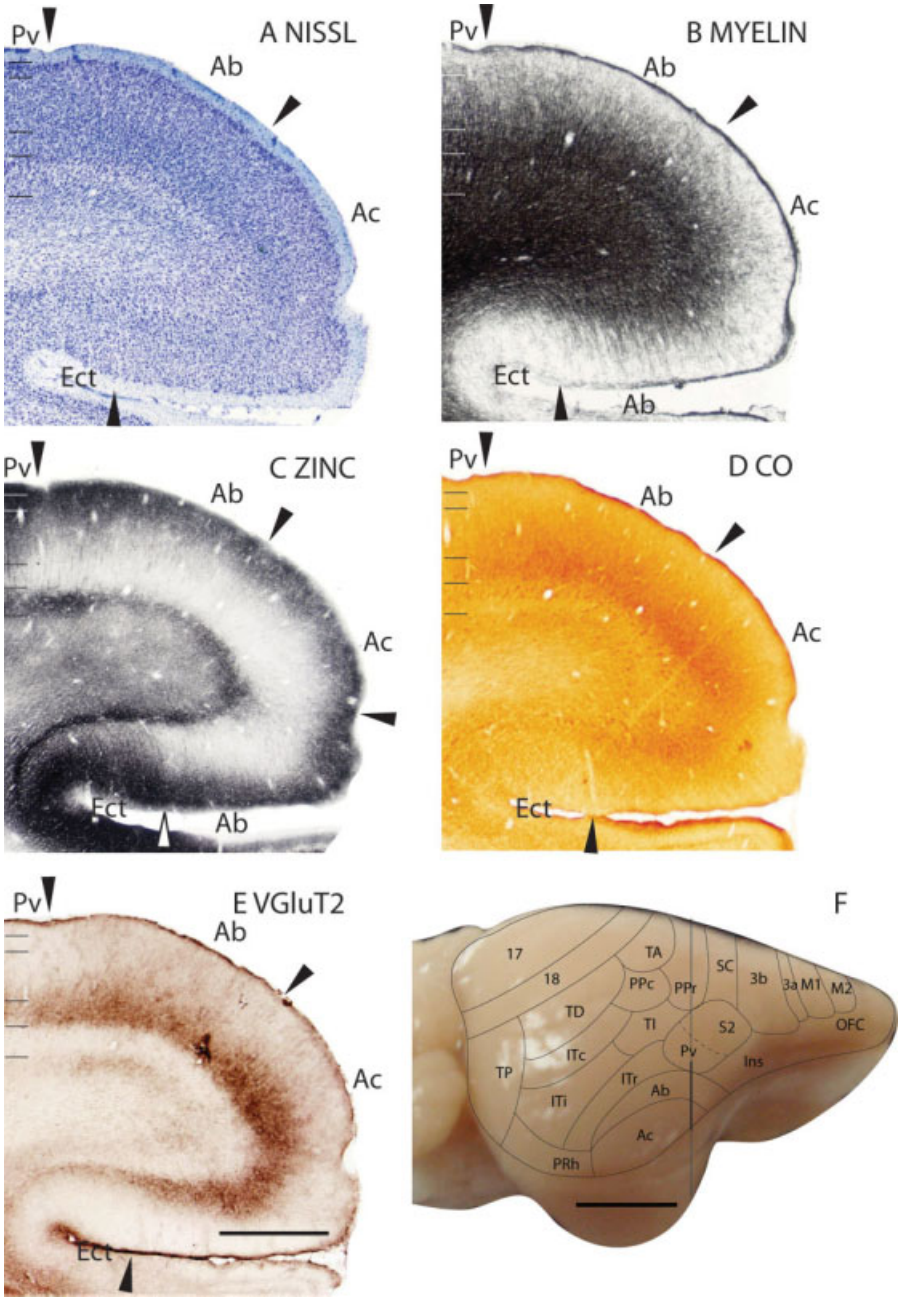

Fig. 12. Architectonic characteristics of the auditory areas. Cortical areas are shown on a lateral view of the right hemisphere in panel **F**. The thicker part of the vertical line across the brain indicates the location of the coronal brain sections illustrated in panels **A**–**E**. Short horizontal lines on panels A to F indicate the extent of the six cortical layers. The scale bar for brain sections (panel E) = 1 mm. The scale bar on the brain (panel F) = 5 mm.

staining compared with Ac (Fig. 12E). Layer 4 of Ab stains darkly for PV-immunopositive terminations, and darkly stained neurons are present throughout the cortical layers (Fig. 13A). The Ab/ITr border is marked by a decrease in PV staining in layer 4 of ITr. The Ab/Ac border is not distinct in the PV stain, although PV staining in layer 4 of Ab is more diffuse than in Ac (Fig. 13A). In sections stained for the SMI-32 antibody, Ab has similar staining characteristics to Ac, with a dense population of SMI-32-immunopositive pyramidal cells in layer 3, and some stained pyramidal cells in layer 5 (Fig. 13B).

Parietal Cortex

The parietal cortex in tree shrews consists of six main areas. Three of these areas are in the anterior parietal cortex: the primary somatosensory area [3b(S1)], the adjoining strip of the transitional area, area 3a, and the

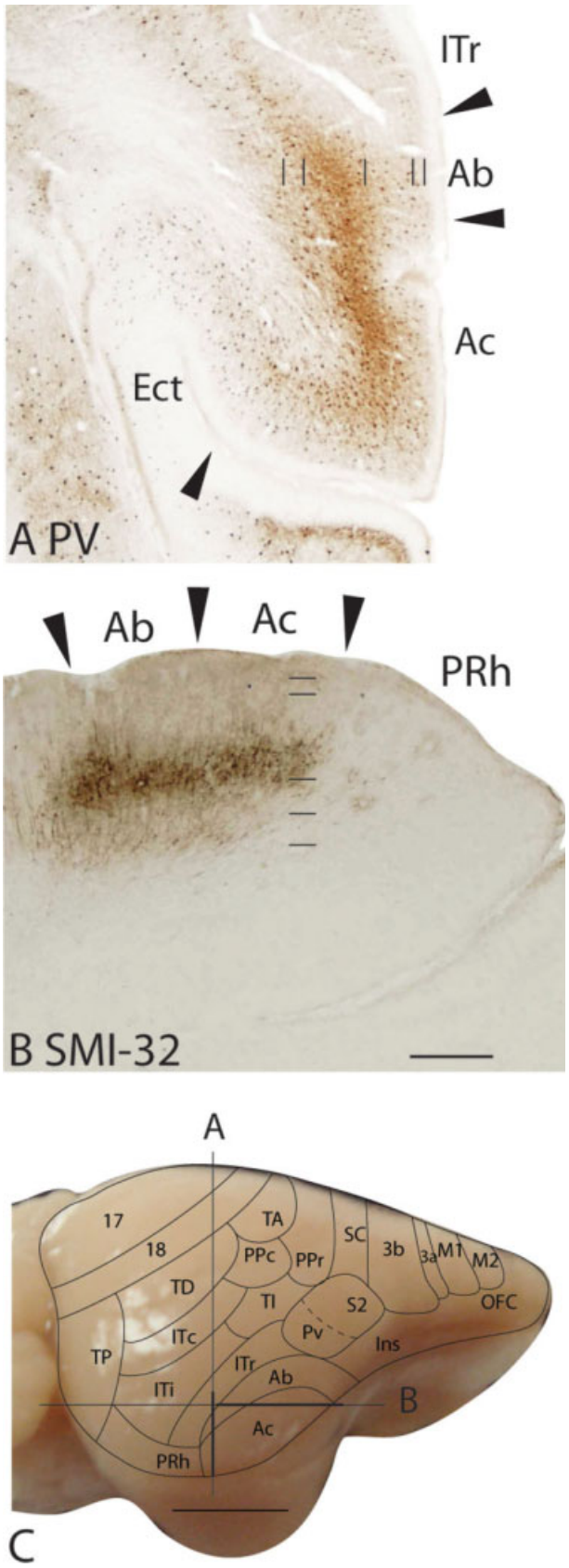

somatosensory caudal area (SC). In the lateral ventral cortex, there are the second somatosensory (S2) and the parietal ventral (Pv) areas. The sixth area is the PP area, which has been subdivided into the posterior parietal dorsal (PPd), posterior parietal rostral (PPr), and PPc areas.

Primary somatosensory area. Area 3b(S1) in tree shrews contains the complete representation of the body, and extends over the medial wall where it abuts the cingulate cortex (Sur et al., 1981b) (for example see Fig. 18D). In Nissl preparations, 3b(S1) has a koniocellular appearance, with a layer 4 that is more densely populated with small granule cells than the surrounding cortical areas, and a layer 5 that is populated with medium-sized pyramidal cells (Figs. 14A, 16A, 17A). In some sections, the thickness of layer 4 in 3b(S1) is not constant throughout the area, and this is observed in the myelin stain as well. 3b(S1) is well myelinated, with two distinct bands of Baillarger, compared with the adjacent areas SC (Fig. 14B), 3a (Figs. 16B, 17B), and the dorsal cingulate area (CGd) (Fig. 16B). However, in favorable sections, the myelinated bands are discontinuous (Fig. 16B). In the zinc stain, 3b(S1) expresses less free zinc ions throughout the cortical layers than the surrounding areas, especially layer 4 of 3b(S1), which appears as a white band, allowing 3b(S1) to be delineated from the adjacent areas such as 3a (Figs, 16C, 17C), SC, and CGd (Figs. 14C, 17C), where layer 4 of those areas stain darker in the zinc stain. The varying thickness of layer 4 in 3b(S1) is observed in the zinc stain as well, forming a "scallop" pattern that is absent in the adjoining insular area (Fig. 16C). The nonuniform thickness of layer 4 that is observed in the Nissl, myelin, zinc, and VGluT2 stain may be due to the presence of different representations of body part in a single section. Layer 4 of 3b(S1) expresses more CO than the adjoining SC and CGd (Fig. 14D), and some darkly stained cell bodies are present in layer 5 (Fig. 14D, 16D).

In the VGluT2 stain, layer 4 of 3b(S1) is darkly stained compared with the surrounding areas SC, CGd (Fig. 14E), and 3a (Figs. 14E, 16E), and the staining is not uniform throughout its extent (Fig. 16E). A lighter stained band is observed in layer 6. Layer 4 of 3b(S1) stains darkly for PV-immunopositive terminations, and a concentration of PV-immunopositive cells is observed in the upper cortical layers (Fig. 17D). In SMI-32 preparations, two bands of pyramidal neurons are labeled in layers 3 and 5 (Fig. 17E). These SMI-32-immunopositive neurons are not as densely packed as those in SC (Fig. 17E) and are smaller than those in 3a (Fig. 17E).

Area 3a. In Nissl preparations, area 3a has a layer 4 that is thinner than in 3b(S1) and is thicker than in M1 (Figs. 16A, 17A). Layer 5 of 3a is populated with pyramidal cells that are larger than those in 3b(S1), but

Fig. 13. Architectonic characteristics of the auditory areas in PV and SMI-32 preparations. Cortical areas are shown on a lateral view of the right hemisphere in panel **C**. The vertical line indicates the location from which the coronal section in panel **A** is taken, and the horizontal line indicates the location from which the horizontal section in panel **B** is taken. The scale bar for brain sections (panel B) = 0.5 mm. The scale bar on the brain (panel **F**) = 5 mm.

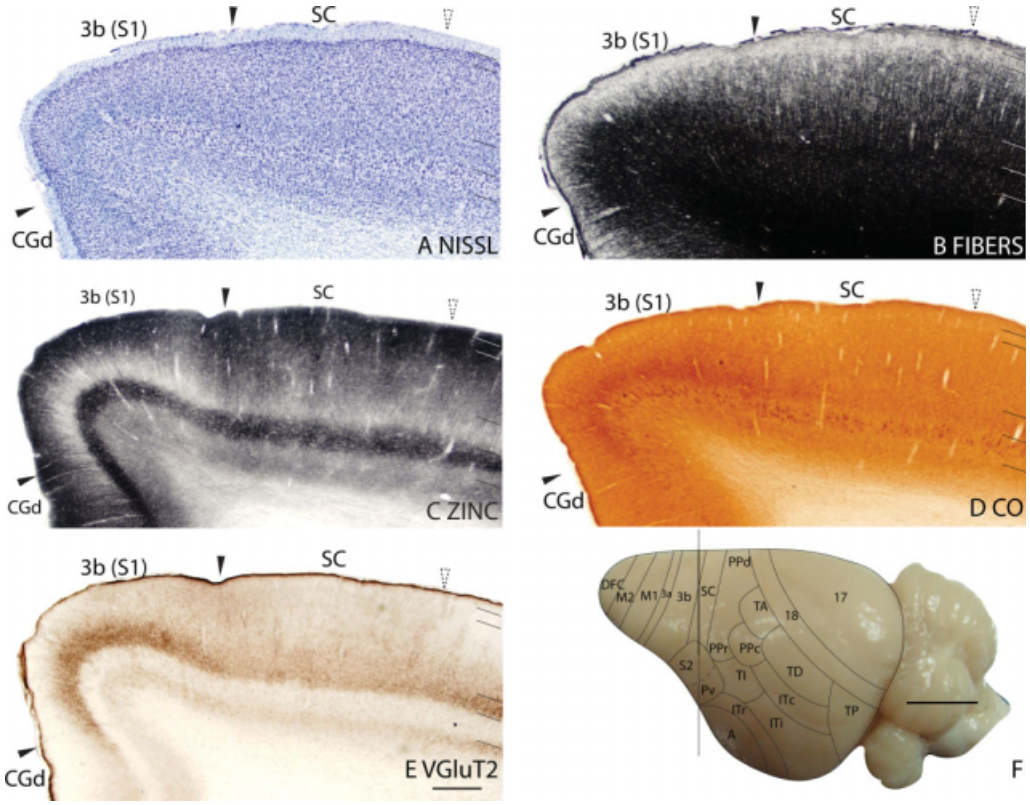

Fig. 14. Architectonic characteristics of the primary somatosensory cortex. Cortical areas are shown on a dorsolateral view of the right hemisphere in panel **F**. The vertical line across the cortex (panel F) indicates the location where the coronal brain sections in panels **A–E** were obtained. Short horizontal lines on panels A–E indicate the extent of the six cortical layers. Solid arrows mark the extent of 3b(S1). Dotted arrows indicate the approximate location of the border between SC and S2. The scale bar for brain sections (panel E) = 0.5 mm. The scale bar on the brain (panel F) = 5 mm.

smaller than in M1 (Figs. 16A, 17A). Although 3a is not as well myelinated as 3b(S1) (Figs. 16B, 17B), an outer band of Baillarger, which is lighter than that in 3b(S1), is present in 3a and absent in M1 (Fig. 17B). Layer 4 of 3a stains darker in the zinc stain than in 3b(S1), and 3a expresses more free zinc ions throughout the cortical layers compared with M1 and 3b(S1) (Figs. 16C, 17C). In CO preparations, darkly stained cell bodies are present in layer 5 of 3a (Fig. 16D).

In VGluT2-immunostained sections, layer 4 of 3a has reduced staining compared with layer 4 of 3b(S1) and has darker staining than layer 4 of M1 (Fig. 16E). No VGluT2 staining is observed in layer 6 of 3a. There are few PV-immunopositive neurons present in area 3a, and the PV-immunopositive terminations that are present in 3b(S1) are absent in 3a (Fig. 17D). In SMI-32 preparations, layer 3 of 3a has fewer, though larger, stained pyramidal neurons than layer 3 of 3b(S1) (Fig. 17E). SMI-32-immunopositive neurons in layer 5 of 3a are larger than those in 3b(S1), but smaller and have shorter apical dendrites than those in M1 (Fig. 17E).

Somatosensory caudal area. In Nissl-stained sections, SC has a moderately packed layer 4 that is thinner than layer 4 of 3b(S1) (Figs. 14A, 17A). Layer 4 of SC is also thinner and packed with smaller cells than layer 4 of S2 (Fig. 15A). Layer 5 of SC is moderately populated with pyramidal cells that are larger than those in 3b(S1) (Figs. 14A, 17A) and PPd (Fig. 17G), but smaller than those in S2 (Fig. 15A). In the myelin stain, SC lacks distinct bands of Baillarger and has reduced myelination compared with 3b(S1) (Figs. 14B, 17B). SC is also not as well myelinated as S2 (Fig. 15B), but has similar levels of myelination to PPd (Fig. 17H). In the zinc stain, SC stains darker, especially in layer 4, compared with both 3b(S1) (Figs. 14C, 17C) and S2 (Fig. 15C), and stains at a similar level to PPd (Fig. 17I). Layer 4 of SC expresses less CO than layer 4 of 3b(S1) (Fig. 14D) and S2 (Fig. 15D), and layer 5 of SC is populated with CO-stained cells (Figs. 14D, 15D).

SC stains lighter in the VGluT2 stain compared with 3b(S1) (Fig. 14E) and S2 (Fig. 15E). A faint band of VGluT2 staining that is present in layer 6 of SC is absent in S2 (Fig. 15E). In PV preparations, PV-immunopositive terminations in SC do not form a dark band in layer 4 as they do in 3b(S1) (Fig. 17D). There is a sparse distribution of PV-immunostained cell bodies in SC, and there is no distinct difference in PV staining between SC and PPd (Fig. 17J). Layer 3 of SC is more densely populated with SMI-32-immunopositive neurons compared with 3b(S1), and in layer 5, the SMI-32-immunopositive pyramidal neurons are larger and more darkly stained than those in 3b(S1) (Fig. 17E) and PPd (Fig. 17K).

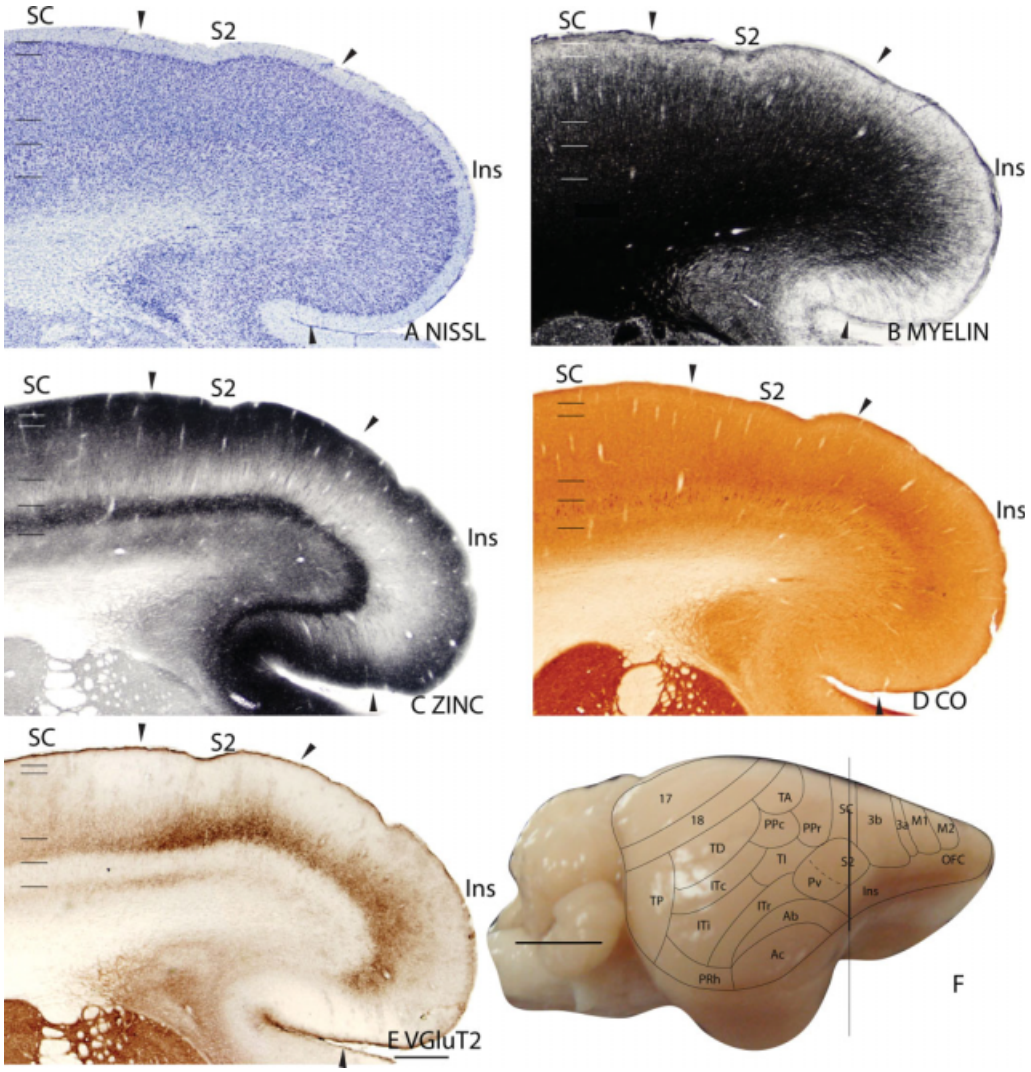

Fig. 15. Architectonic characteristics of the secondary somatosensory cortex and insular cortex. Cortical areas are shown on a lateral view of the right hemisphere in panel **F**. The vertical line across the cortex (panel F) indicates the location where the coronal brain sections in panels **A–E** were obtained. The extent of each cortical layers 1 to 6 is indicated by the short horizontal lines on panels A–E. The scale bar for brain sections (panel E) = 0.5 mm. The scale bar on the brain (panel F) = 5 mm.

Second somatosensory and parietal ventral areas. S2 in tree shrews contains a topographic map of the contralateral body surface, and cortex caudal and lateral to S2, which corresponds to Pv, is also responsive to somatosensory stimulation (Sur et al., 1981a). Remple et al. (2006) distinguished Pv from S2 in the Nissl stain, where in Pv, layer 5 was thinner and more densely packed compared with S2. In the other stains used, S2 and Pv have similar patterns of staining. Results presented here for S2 also apply to Pv, as we did not distinguish an architectonic border between the two fields.

In Nissl-stained sections, S2 has a well-developed layer 4 that is thinner than that of 3b(S1) and thicker than that of SC. Layer 5 of S2 is populated with pyramidal cells that are larger than the adjoining insular (Ins) area (Fig. 15A), but are smaller than in 3b(S1). S2 is more highly myelinated than SC but is less myelinated than Ins (Fig. 15B). No bands of Baillarger are observed in S2 (Fig. 15B). In the zinc stain, layer 4 of S2 is lighter stained than in SC (Fig. 15C), but is darker stained than in 3b(S1) and Ins (Fig. 15B). Layers 1 to 3 of S2 also express more free zinc ions than Ins (Fig. 15C). Layer 4 of S2 is thinner and stains less intensely for CO than layer 4 of Ins (Fig. 15D).

In VGluT2 preparations, a band of VGluT2-immunostained terminations in layer 4 of S2 is thinner and darker than in Ins, and thicker and darker than in SC (Fig. 15E). No VGluT2 immunostaining is observed in layer 6 of S2. Layer 4 of S2 has reduced staining of PV-immunopositive terminations compared with 3b(S1) and Ins, and has higher staining compared with SC (not shown). In SMI-32 preparations, the pyramidal cells in layer 3 of S2 are less darkly stained, and the pyramidal cells in layer 5 are smaller than those in 3b(S1) (not shown).

Posterior parietal area. The PP area has been divided into three regions, PPr, PPc, and PPd, where each of these regions has different connections patterns with the motor cortex (Remple et al., 2007). Although areas PPd and PPr have dissimilar connection patterns with the motor cortex, they have similar architectonic characteristics, and we were unable to reliably determine the architectonic border between them. As such, they were drawn as a single architectonic field in our summary diagrams.

In Nissl-stained sections, layer 4 of PPd is thicker and more populated with granule cells than the adjoining TA (Fig. 5A), but is neither as well developed nor as populated with granule cells when compared with area infraradiata dorsalis (IRd) along the medial wall (Fig. 20A). Layer 5 of PPd has a similar packing density of pyramidal cells compared with TA (Fig. 5A), and a reduced packing density compared with area 18 and SC (Fig. 17G). Pyramidal cells in layer 5 are larger than those in area 18 and SC (Figs. 5A, 17G), and similarly sized to those in TA (Fig. 5A). PPd also has a higher packing density of cells in layers 1 to 3 compared with TA (Fig. 5A). In myelin preparations, PPd has similar myelination levels as SC (Fig. 17H) and is less myelinated than area 18, TA (Fig. 5B), and IRd (Fig. 20B). PPd expresses free zinc ions throughout the cortical layers. Layers 1 to 3 are darker in the zinc stain than the corresponding layers in TA (Fig. 5C), and layer 5 stains lighter for free zinc ions than IRd (Fig. 20D). In CO preparations, layer 4 of PPd is not darkly stained, and layer 5 is populated with darkly stained cell bodies (Fig. 20F).

PPd shows reduced staining for VGluT2-immunopositive terminals compared with the surrounding areas, such as SC and area 18, except for IRd, where the staining intensities in layer 4 are similar (Fig. 20E). In PV preparations, the staining intensities of PPd, TA (Fig. 5D), and SC (Fig. 17J) are similar. The PPd/IRd border is distinct in PV-stained sections, as PV-immunopositive terminations are absent in layer 4 of PPd and are present in layer 4 of IRd (Fig. 20C). PPd and TA have similar staining characteristics in the SMI-32 stain, where there is dense staining in layer 3, and layer 5 is populated with medium-sized pyramidal cells (Fig. 5E). The SMI-32-immunostained pyramidal cells in layer 3 of PPd have smaller apical dendrites than in area 18 (Figs. 5E, 17K), and in layer 5, PPd is more densely populated with SMI-32-immunopositive pyramidal cells than area 18 (Figs. 5E, 17K).

In Nissl-stained sections, layer 4 of PPc is populated by small granule cells, and layer 5 is populated by medium-sized pyramidal cells that are mainly in outer layer 5 (Fig. 11A). PPc has reduced myelination compared with TD and TI, and no bands of Baillarger are observed (Figs. 6B, 11B). In the zinc stain, PPc stains darker for zinc than TI (Fig. 11C), and stains at similar intensity to ITc and TA (Fig. 6D). CO staining in layer 4 of PPc is lower than in TI, and in layer 5, darkly stained cell bodies are present (Fig. 11D).

Layer 4 of PPc shows diffuse and less intense staining for VGluT2 antibody compared with TI (Fig. 11E). PPc also stains less intensely for PV compared with the surrounding areas (Fig. 6E), and a sparse population of SMI-32-immunostained pyramidal cells is observed in layer 5 of PPc (not shown).

Frontal Cortex

Here, the frontal cortex in tree shrews is divided into four areas, the primary motor area (M1), the secondary motor area (M2), the dorsal frontal cortex (DFC), and the orbital frontal cortex (OFC).

Primary motor cortex. M1 is a narrow strip, ~1 mm wide, that has a complete body and orofacial representation (Remple et al., 2006). In the Nissl stain, M1 has a poorly developed layer 4, and a well-developed layer 5, where inner layer 5 is populated with large pyramidal cells (Figs. 16A, 17A). M1 is less well myelinated than 3a, with no distinct band of Baillarger (Figs. 16B, 17B), and has similar levels of myelination to M2 (Fig. 17B). In the zinc stain, the staining intensity is lower in M1 than in M2 (Fig. 17C) and MMA (Fig. 16C), and higher, especially in layer 4, than in 3a and 3b(S1) (Figs. 16C, 17C). M1 does not express high levels of CO in layer 4 (Fig. 16D), although darkly stained cell bodies are observed in layer 5.

In VGluT2 preparations, layer 4 of M1 stains poorly compared with 3a, but is darker stained than MMA (Fig. 16E). No VGluT2 staining is observed in layer 6 of M1. In the PV stain, M1 stains poorly for PV-immunopositive terminations and is sparsely populated with PV-immunopositive neurons (Fig. 17D). M1 has large, densely stained SMI-32 pyramidal neurons in layer 5, with thick apical dendrites that extend to layer 3 (Fig. 17E). No SMI-32-immunopositive neurons were present in layer 3 of M1.

Secondary motor cortex. M2 is delineated from M1 by a thinner layer 5 that is less densely packed with pyramidal neurons than in M1 (Fig. 17A). The M2/DFC border is marked by the return of a granular layer 4 and smaller layer 5 pyramidal cells in DFC (Figs. 17A, 18A). In myelin preparations, M2 is more myelinated than DFC (Figs. 17B, 18B) and less myelinated than OFC (Fig. 18B). M2 expresses higher levels of free zinc ions throughout the cortical layers compared with the adjacent cortical areas such as M1 (Fig. 17C), DFC (Figs. 17C, 19A), and OFC (Fig. 19A). In CO preparations, the rostral border of M2 with DFC is not distinct, except for the larger sized, darkly stained cell bodies in layer 5 of M2 than in layer 5 of DFC (Fig. 19C). The M2/OFC border is distinct in CO preparations, as a band of dark CO staining is present in layer 4 of OFC and absent in M2 (Fig. 19C).

M2 expresses low levels of VGluT2 staining, resulting in a distinct M2/OFC border (Fig. 19B). The rostral border of M2 with DFC is not as distinct in VGluT2 preparations, as both cortical areas stain at similar intensities (Fig. 19B). No VGluT2 staining is observed in layer 6 of M2. PV staining in M2 is lower than in DFC and OFC (Fig. 18C) and is similar to that of M1 (Fig. 17D). SMI-32-immunoreactive pyramidal cells in layer 5 of M2 were smaller than those in M1 and had thinner apical dendrites (Fig. 17E). No SMI-32-immunoreactive pyramidal cells are observed in layer 3 of M2. The M2/DFC border is marked by a transition to a sparser population of small SMI-32-immunoreactive cells, with poorly stained cell bodies and thin apical dendrites (Fig. 17E).

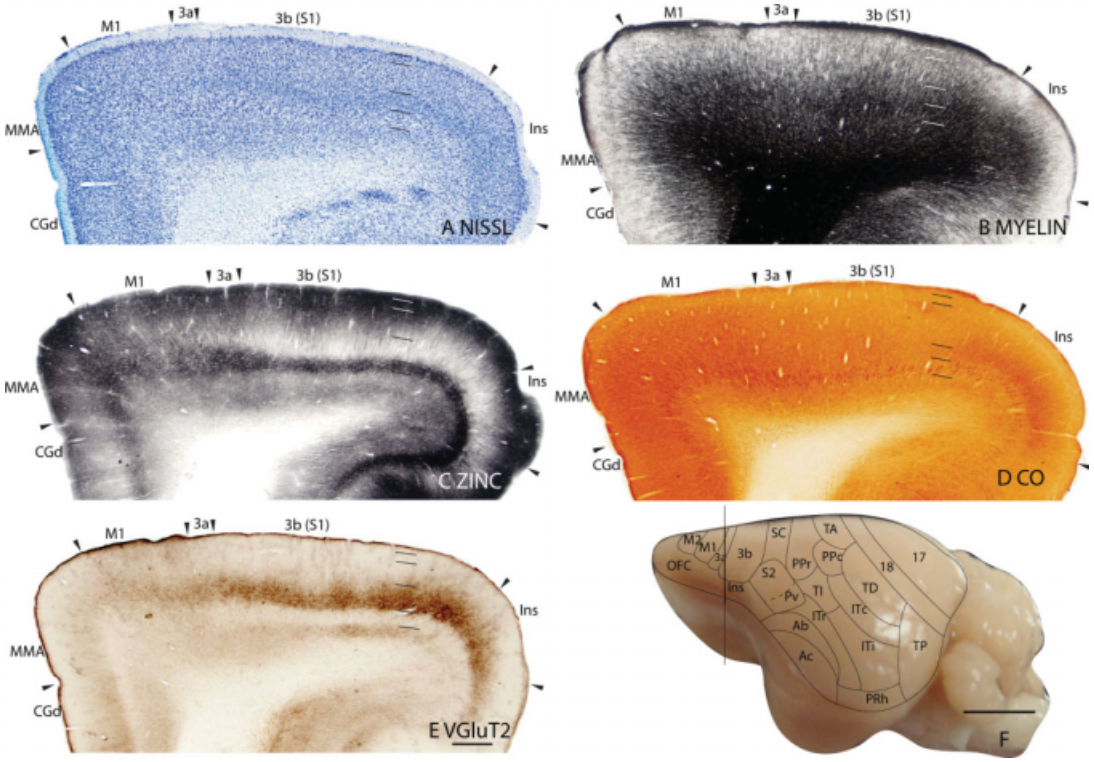

Fig. 16. Architectonic characteristics of primary somatosensory and motor areas. Cortical areas are shown on a lateral view of the left hemisphere in panel **F**. The vertical line across the cortex (panel F) indicates the location where the coronal brain sections in panels **A–E** were obtained. Short horizontal lines on panels A–E indicate the extent of the six cortical layers. The scale bar for brain sections (panel E) = 0.5 mm. The scale bar on the brain (panel F) = 5 mm.

Dorsal frontal cortex. In Nissl-stained sections, DFC has a thin granular 4 (Figs. 17A, 18A). DFC also has a lower cell packing density throughout the cortical layers, resulting in a paler appearance of DFC compared with the medial frontal (MF) area (Fig. 18A). In myelin preparations, DFC has reduced myelination compared with the surrounding areas such as M2 and MF (Figs. 17B, 18B). DFC has lower expression of free zinc ions compared with M2, especially in layer 4 (Fig. 19A). However, the zinc staining of layer 4 in DFC is not homogenous as it reduces toward the DFC/MF border, which is marked by the transition to increased zinc stain in layer 4 of MF (Fig. 18A). There is no band of CO staining in layer 4 of DFC, although there are darkly stained cell bodies in layer 5 (Fig. 19C). This allows for the demarcation of the DFC/MF border, where there is a band of CO staining in layer 4 of MF (Fig. 19C).

VGluT2 expression in DFC is similar to that of M2 and MF; as such the borders of DFC are not distinct in the VGluT2 stain (Fig. 19B). In PV preparations, a thin, PV-stained band is observed in layer 6 of DFC (Fig. 18C). Layers 3 to 5 of DFC stains darker for PV-immunopositive terminals compared with M2 and MF, and DFC has a larger population of PV-immunopositive neurons than M2 (Fig. 18C). In SMI-32 preparations, DFC does not have stained pyramidal cells in layer 3, and has a sparse population of poorly stained pyramidal cells bodies in layer 5 that have thin apical dendrites (Fig. 17E).

Orbital frontal cortex. In Nissl preparations, OFC is overall more densely populated with cells than M2, giving it a darker appearance than M2 (Fig. 18A). OFC has a well-developed layer 4 that is populated with small granule cells (Fig. 18A). Layer 5 of OFC has a lower cell packing density and is populated with smaller pyramidal cells than layer 5 of M2 (Fig. 18A). The ventral border of OFC is marked by a transition to poorly laminated cortex with a thick, densely populated layer 2/3 in the claustral cortex (Cl) (Fig. 18A). OFC is more myelinated than the surrounding cortical areas M2 and Cl (Fig. 18B). In zinc preparations, layer 4 of OFC stains poorly, standing out as a white band. As a result, a distinct dorsal border with M2 and ventral border with Cl is seen in the zinc stain, as layer 4 both of the adjoining areas expresses higher levels of free zinc ions (Fig. 19A). Layer 4 of OFC stains darkly in CO preparations, expressing higher levels of CO protein than the surrounding areas M2 and Cl (Fig. 19C).

OFC has a darkly stained VGluT2-immunopositive band in layer 4 that terminates at the OFC/M2 and OFC/Cl borders (Fig. 19B). In PV preparations, OFC has darker PV staining compared with M2, with an increased population of PV-immunoreactive neurons throughout the cortical layers. OFC also has a band of PV-immunopositive terminations in layer 4 and a thinner band in layer 6 (Fig. 18C). The upper cortical layers of OFC are less darkly stained than in Cl (Fig. 18C). In SMI-32 preparations, there are no immunostained

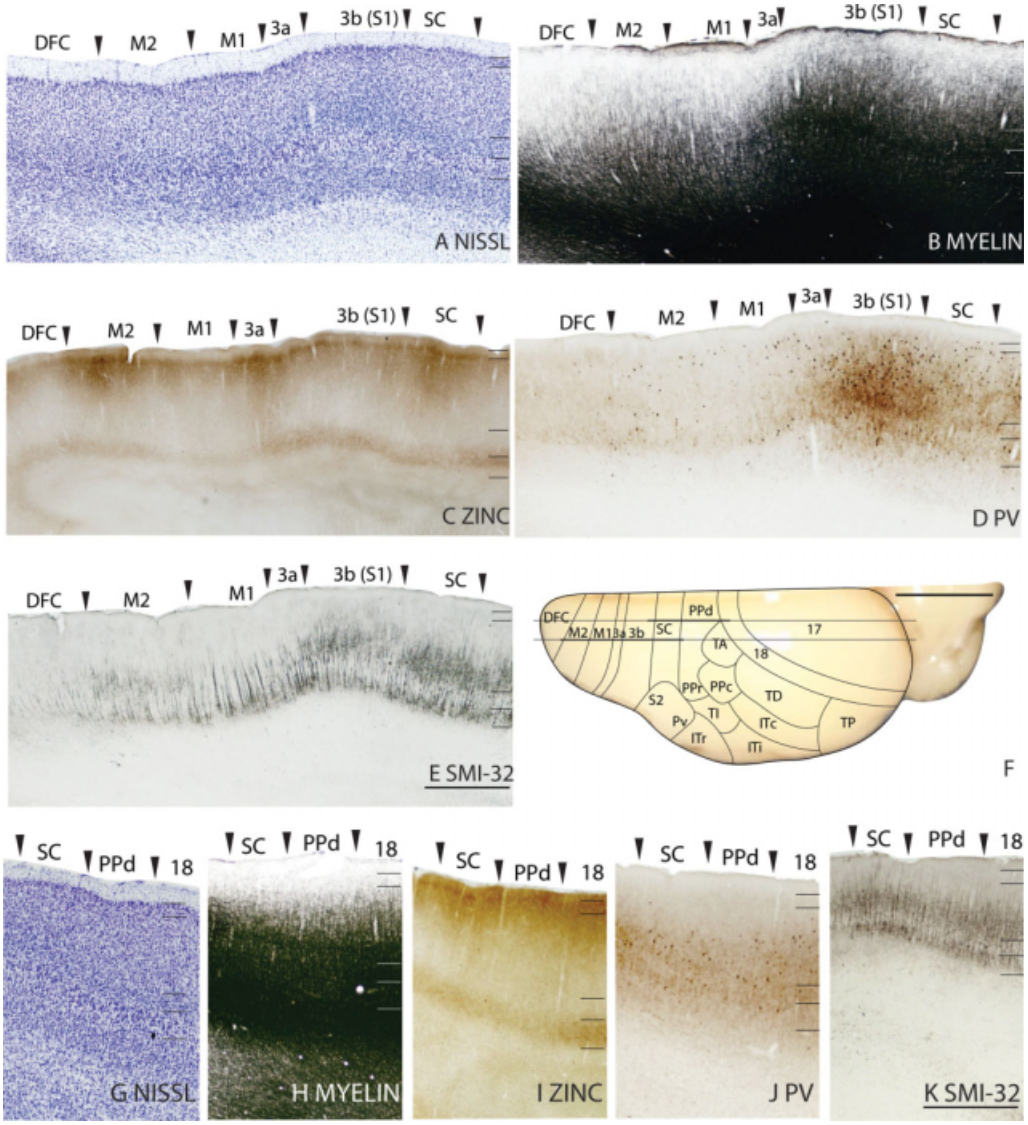

Fig. 17. Architectonic characteristics of somatosensory and motor areas. Cortical areas are shown on a dorsal view of the left hemisphere in panel **F**. The lateral most horizontal line across the cortex (panel F) indicates the location where the sagittal brain sections in panels **A–E** were obtained. The horizontal line across the cortex (panel F) that is close to the medial wall indicates the location where the sagittal brain sections in panels **G–K** were obtained. The scale bar for brain sections (panels E and K) = 1 mm. The scale bar on the brain (panel F) = 5 mm.

pyramidal cell bodies, and some short immunostained dendrites in OFC (not shown).

Medial Cortex

The cortical areas along the medial wall of the tree shrew neocortex can be divided into rostral, middle, and caudal regions. The rostral region consists of the MF, the CGd, the ventral cingulate (CGv), and the medial motor (MMA) areas. In tree shrews, the somatosensory cortex, including areas 3a, 3b(S1), and SC, wraps onto the medial wall to occupy part of the middle region, and the rest consists of the infraradiata areas. The caudal region, largely occupied by area 17, also includes area 18, PS, and the retrosplenial areas.

Medial frontal area. In Nissl preparations, MF has a well-developed layer 4 that is more densely populated with granule cells than in DFC, and a layer 5 that is less densely populated with cells than in CGv (Fig. 18A). MF is also more heavily myelinated than DFC and CGv (Fig. 18B). In the zinc stain, MF expresses more free zinc ions in layer 4 than DFC, with a higher density of zinc stained "strings" running through layer 4 (Fig. 19A). MF has a band of CO staining in layer 4 that is absent in both DFC and CGv (Fig. 19C) and darkly stained cell bodies in layer 5.

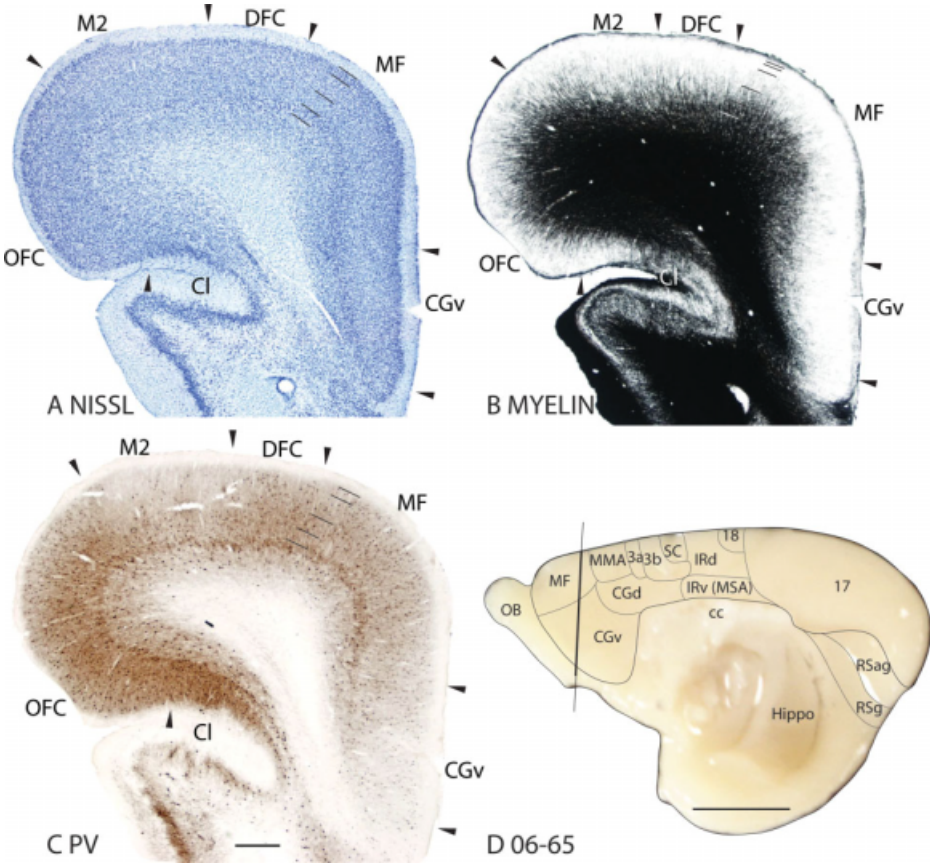

Fig. 18. Architectonic characteristics of the medial frontal and cingulate areas. Cortical areas are shown on the medial view of the right hemisphere (panel **D**). The vertical line across the cortex (panel D) indicates the location where the coronal brain sections in panels **A**–**C** were obtained. The extent of each cortical layers 1 to 6 is indicated by the short horizontal lines on panels A–C. The scale bar for brain sections (panel **E**) = 0.5 mm. The scale bar on the brain (panel **F**) = 5 mm.

The borders of MF in the VGluT2 stain are not distinct as the adjoining cortical areas, DFC and CGv, stain with similar intensities to MF for the VGluT2 stain (Fig. 19B). In PV preparations, a thin band of PV stain is present in layer 6, and darkly stained PV-immunopositive cell bodies are present throughout the cortical layers (Fig. 18C). There is no distinct difference between DFC and MF in the PV stain, whereas the MF/CGv border is marked by a transition to a sparser distribution of PV-immunopositive cell bodies and the absence of PV stain in layer 6 of CGv.

Cingulate ventral area. CGv has a less densely populated, and a thinner layer 4 than MF in Nissl-stained sections (Fig. 18A). The upper cortical layers 2 and 3 are populated with larger cells than in MF, although this changes in the ventral portion of CGv, where the cells that populate layer 2 and 3 are reduced in size (Fig. 18A). Layer 5 of CGv is thick and densely populated with cells. In myelin preparations, CGv is less myelinated than MF (Fig. 18B). The pattern of zinc staining in CGv is not homogenous. At the dorsal border of CGv, layer 4 stains very poorly for the zinc stain, and the staining increases toward the ventral border of CGv (Fig. 19A). CGv stains poorly for CO (Fig. 19C). The variable staining patterns in the Nissl and zinc stains suggest the possibility for further subdividing CGv.

CGv stains poorly in the VGluT2 stain (Fig. 19B). In the PV stain, no dense bands of PV-immunopositive terminations are observed, and only a scattering of small PV-immunopositive cell bodies are present (Fig. 18C).

Cingulate dorsal area. CGd is densely populated with cells throughout the cortical layers, giving it a dark appearance in the Nissl stain (Fig. 16A). Layer 4 in CGd is very thin and not well developed, and layer 5 is densely populated with small pyramidal cells. The 3b(S1)/CGd border is marked by the reduction in the thickness of layer 4 in CGd (Fig. 14A). CGd is less heavily myelinated than MMA (Fig. 16B) and 3b(S1) (Fig. 14B). In the zinc stain, CGd stains more intensely than 3b(S1) (Fig. 14C), especially in layer 4, where CGd expresses more free zinc ions than layer 4 of 3b(S1). CGd expresses less free zinc ions than MMA, as such CGd has a lighter appearance than MMA in zinc-stained sections (Fig. 16C). In CO preparations, the CGd/3b(S1) border is marked by the reduction of CO staining in CGd (Fig. 14D).

CGd has reduced expression of VGluT2-immunopositive terminals compared with 3b(S1), resulting in a

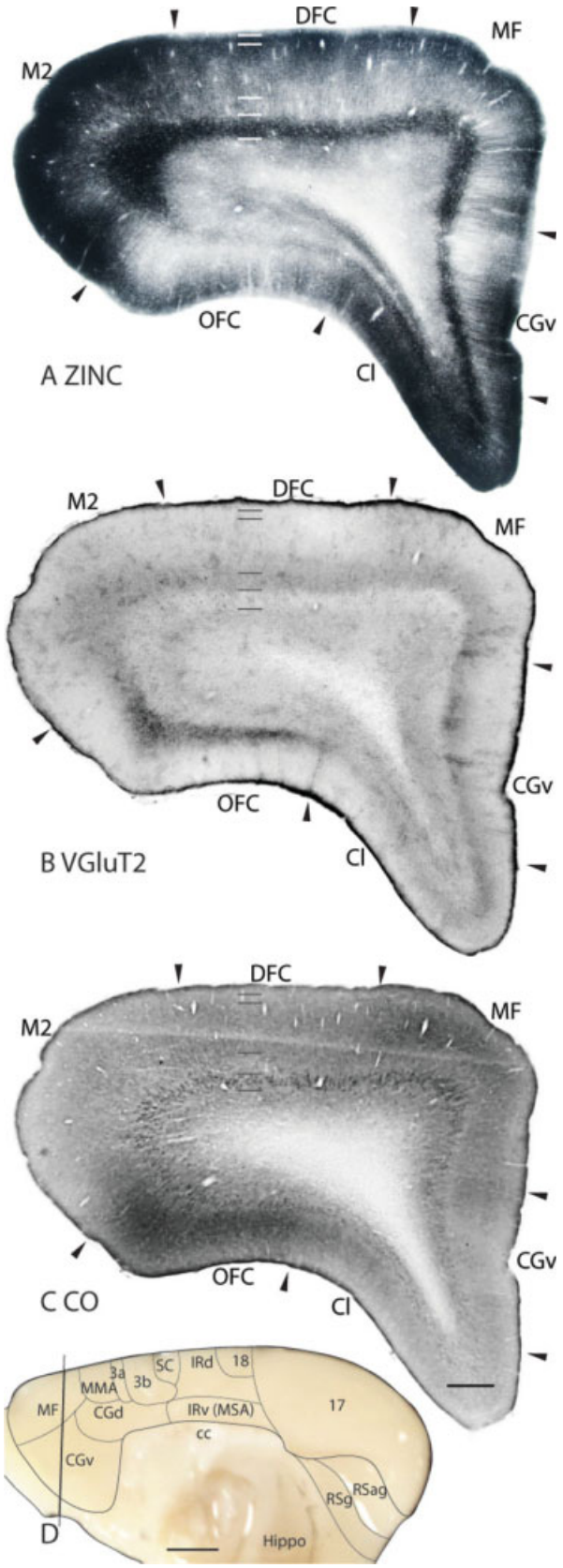

distinct 3b(S1)/CGd border (Fig. 14E). The CGd/MMA border is not as distinct, although CGd stains more intensely for VGluT2 than MMA (Fig. 16E). In the PV stain, the dorsal border of CGd with 3b(S1) is marked by a transition to reduced PV staining in CGd and the absence of PV-immunopositive terminals in layer 4 of CGd (not shown). The PV staining pattern of CGd is similar to that of CGv.

Medial motor area. MMA is adjacent to M1 along the medial wall and has projections to M1 and M2 (Remple et al., 2007). MMA does not have a distinct granular layer 4 and has a thick layer 5 that is densely populated with pyramidal cells (Fig. 16A). The upper cortical layers 2 and 3 of MMA are densely populated with cells, giving it a darker appearance than the adjacent M1 (Fig. 16A). MMA is as heavily myelinated as M1 and is more heavily myelinated than CGd (Fig. 16A). In the zinc stain, MMA expresses more free zinc ions throughout its cortical layers than both CGd and M1 (Fig. 16C). MMA stains poorly for CO, and it is difficult to define the MMA/CGd and M1/MMA borders in CO preparations (Fig. 16D)

In VGluT2 preparations, layer 4 of MMA stains less densely than the surrounding areas (Fig. 16E), and PV expression in terminals is weak, with a sparse scattering of PV-immunopositive neurons (not shown).

Infraradiata dorsal area. In Nissl preparations, layer 4 of IRd is sparsely populated with medium-sized cells, and layer 5 is sparsely populated with small pyramidal cells (Fig. 20). IRd is myelinated at similar levels to PPd, and is more heavily myelinated than the infraradiata ventral area (IRv) (Fig. 20B). In the zinc stain, IRd expresses more free zinc ions in layers 4 and 5 compared with PPd (Fig. 20D). The borders of IRd are not as obvious in the CO stain as the CO expression of IRd, and the adjoining PPd and IRv are similar (Fig. 20F).

Reduced VGluT2 staining intensity in IRd marks the IRd/IRv border (Fig. 20E). However, IRd has similar levels of VGluT2 staining to PPd, as such the IRd/PPd border is not distinct in VGluT2 preparations (Fig. 20E). In PV preparations, IRd is more darkly stained than PPd, and layer 4 of IRd is more darkly stained with PV-immunopositive terminals than layer 4 of PPd (Fig. 20C).

Infraradiata ventral area. In Nissl-stained sections, IRv has a thin layer 4, and a layer 5 that is more densely populated with small cells than IRd (Fig. 20A). IRv is less heavily myelinated than IRd, and an outer band of Baillarger is present (Fig. 20B). The upper cortical layers 2 and 3 and layer 5 of IRv stain darker in the zinc stain than the corresponding layers in IRd (Fig. 20D). The ventral border of IRv is marked by a reduced

Fig. 19. Architectonic characteristics of the medial frontal and cingulate ventral area. Cortical areas are shown on the medial view of the right hemisphere (panel **D**). The vertical line across the cortex (panel D) indicates the location where the coronal brain sections in panels A–C were obtained. Short horizontal lines on panels **A**–**E** indicate the extent of the six cortical layers. The scale bar for brain sections (panel C) = 0.5 mm. The scale bar on the brain (panel D) = 2.5 mm.

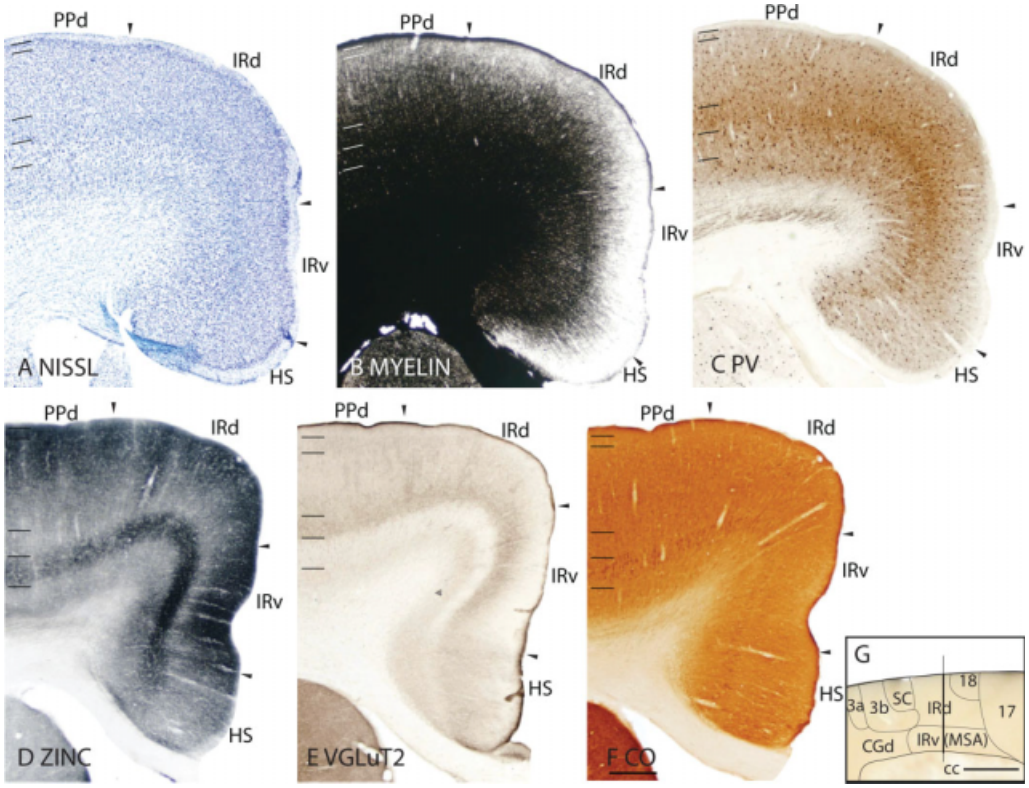

Fig. 20. Architectonic characteristics of the infraradiata areas. Cortical areas are shown on the medial view of the right hemisphere (panel **G**). The vertical line across the cortex (panel G) indicates the location where the coronal brain sections in panels **A–F** were obtained. The extent of each cortical layers 1 to 6 is indicated by the short horizontal lines on panels A–F. The scale bar for brain sections (panel F) = 0.5 mm. The scale bar on the brain (panel G) = 2.5 mm.

expression of free zinc ions. IRv stains lightly for CO (Fig. 20F).

In VGluT2 preparations, two immunostained bands are present in IRv, a darker band in layer 4 and a lighter band in layer 6 (Fig. 20E). Layer 4 of IRv stains darker for VGluT2 than layer 4 of IRd. The absence of the two bands in adjoining cortex marks the ventral border of IRv (Fig. 20E). PV immunostaining in layer 4 of IRv is more diffuse than in IRd, and layers 2 and 3 of IRv do not stain as darkly for PV, giving IRv a paler appearance than IRd (Fig. 20C). IRv expresses more PV staining than the adjoining cortex, allowing the delineation of the ventral border of IRv (Fig. 20C).

Prostriata. PS runs between the ventromedial edge of area 17 and the retrosplenial agranular (RSag) area, where there is a slope in the cortex. In Nissl preparations, the area 17/PS border is marked by a disappearance of a well-developed granular layer 4 in PS (Fig. 2A). Layer 2 of PS is more densely packed with cells than in RSag (Fig. 2A). PS is more lightly myelinated than area 17, and, to a lesser extent, RSag (Figs. 2B, 21A). PS expresses higher levels of free zinc ions throughout the cortical layers compared with the adjoining area 17 and RSag (Figs. 2C, 21B). The absence of a dark CO-stained band in layer 4 marks the transition to PS from area 17 (Fig. 21C).

PS shows almost no VGluT2 staining (Fig. 21D). In PV preparations, a scattering of PV-immunopositive cell bodies is observed (Fig. 21E), and no staining of PV-immunopositive terminations is observed (Figs. 2D, 21E). There are no SMI-32-immunostained cell bodies present in PS (Fig. 2E).

Retrosplenial agranular area. In Nissl preparations, RSag is not well laminated. It has lower cell packing density, and as a result has a paler appearance than the adjoining PS and retrosplenial granular (RSg) areas (Fig. 2A). RSag is lightly myelinated compared with RSg, but is more heavily myelinated than PS (Fig. 21A). In zinc preparations, RSag is more lightly stained than PS, especially in layer 5, and is more darkly stained in layers 1 to 3 than in RSg (Figs. 2C, 21B). CO expression in RSag is poor, and there is no distinct different in staining pattern between RSag and PS (Fig. 21C).

RSag does not have visibly detectable levels of VGluT2 (Fig. 21D) and SMI-32 (Fig. 2E) immunoreactivity. In PV preparations, RSag has a similar staining pattern to PS and has a lighter appearance in layers 1 to 3 when compared with RSg (Fig. 21E).

Retrosplenial granular area. In Nissl preparations, darker staining of layer 2/3 in RSg marks the RSag/RSg border (Fig. 2A). Similar to RSag, RSg does not have well-developed laminar properties. RSg is more

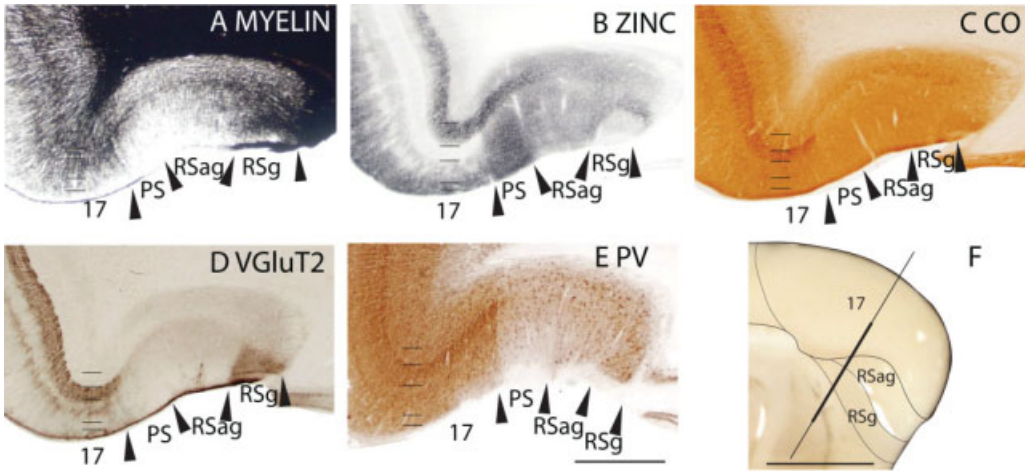

Fig. 21. Architectonic characteristics of the retrosplenial areas. Cortical areas are shown on the medial view of the right caudal hemisphere (panel **F**). The vertical line across the cortex (panel F) indicates the location where the coronal brain sections in panels **A–E** were obtained. The scale bar for brain sections (panel E) = 0.5 mm. The scale bar on the brain (panel F) = 5 mm.

heavily myelinated than RSag (Figs. 2B, 21A). The upper cortical layers 1 to 3 of RSg stain less intensely in the zinc stain than RSag, and no darkly stained band is observed in layer 5 (Fig. 21B). In CO preparations, RSg has poor CO expression (Fig. 21C). However, a denser population of CO stained cell bodies in layer 5 is present in RSg than in RSag (Fig. 21C).

The upper cortical layers 2/3 of RSg stain darkly for VGluT2, providing a sharp border between RSg and RSag (Fig. 21D). In PV preparations, RSg has more darkly stained PV-immunopositive cell bodies than RSag, and RSg has an overall darker appearance than RSag (Fig. 21E). Closer to the rostral border of RSag, SMI-32-immunopositive dendrites are present in the middle layers, and a few SMI-32-immunopositive cell bodies are present in layer 5 of RSag (Fig. 2E).

Remaining Cortical Areas

Insular area. In Nissl preparations, Ins has a well-developed layer 4 that is populated by granule cells that are small than those in S2 (Fig. 15A). Layer 5 of Ins is more sparsely populated with cells than both 3b(S1) and S2, giving it a paler appearance than the adjoining areas (Figs. 1A, 16A). Ins is as heavily myelinated as S2 (Fig. 15B), and is less heavily myelinated than 3b(S1) (Fig. 16B). In zinc preparations, Ins expresses lower levels of free zinc ions throughout the cortical layers than S2 (Fig. 15C). The difference in free zinc ion expression between S2 and Ins is most distinct in layer 4 (Fig. 15C). Ins expresses higher levels of free zinc ions compared with 3b(S1), especially in layer 5 (Fig. 16C). In CO preparations, layer 4 of Ins stains more intensely than in S2 (Fig. 15D).

Layer 4 of Ins contains VGluT2-immunopositive terminations, and no staining is observed in layer 6 (Figs. 15E, 16E). VGluT2 expression in layer 4 of Ins is lower and the staining is more diffuse than in S2 (Fig. 15E), whereas the VGluT2 expression in layer 4 of Ins is less intense than in 3b(S1) (Fig. 16E). In PV preparations, PV staining in layer 4 of Ins is more intense than in S2 and less intense than in 3b(S1) (not shown).

Perirhinal area. In Nissl-stained sections, Prh does not have a well-developed layer 4 and has a low cell population density, giving it a pale appearance (Figs. 7A, 8B, 10A). It is also poorly myelinated compared with the adjoining areas TP, ITr, and the entorhinal cortex (Figs. 7B, 9C, 10B). In zinc preparations, Prh stains more intensely compared with the surrounding areas, such as TP (Fig. 9E) and ITr (Fig. 10C), whereas it stains at similar intensity to the entorhinal cortex (Fig. 9E). Prh stains poorly in the CO stain (Figs. 9D, 10D). In the three immunostains used, Prh has low immunoreactivity for all three, VGluT2 (Fig. 10E), PV (Fig, 7C), and SMI-32 (not shown).

DISCUSSION

In this study, we used a battery of histological procedures to reveal and characterize the architectonic subdivisions of tree shrew neocortex that have known or presumed functional significance. Previous architectonic studies of tree shrews (Le Gros Clark, 1924; von Bonin and Bailey, 1961; Zilles, 1978) have been limited and were completed too early to take advantage of the many immunohistochemical and other architectonic procedures that are now available to help characterize cortical areas. There has been a longstanding (e.g., Le Gros Clark, 1924) and persisting interest in cortical organization of tree shrews (e.g., Kaas et al., 1972; Sesma et al., 1984; Lyon et al., 1998; Remple et al., 2006), as they are close relatives of primates (Liu et al., 2001; Murphy et al., 2001a,b; Springer et al., 2003), and insights into cortical organization in tree shrews should inform theories of forebrain evolution in primates. As the differences between areas reflect functional specializations, we discuss the functional implications of the architectonic differences across cortical fields. Most notably, previous findings indicate that cortical areas with layer 4 terminations that have dense expression of VGluT2 and PV,

and little synaptic zinc are likely to be dominated by thalamic rather than cortical inputs (Van Brederode et al., 1990; DeFelipe and Jones, 1991; de Venecia et al., 1998; Hackett et al., 1998; Latawiec et al., 2000; Cruikshank et al., 2001; Fujiyama et al., 2001; Kaneko and Fujiyama, 2002; Valente et al., 2002; Nahmani and Erisir, 2005; Wong and Kaas, 2008). Areas of high metabolic activity, typically sensory areas, express high levels of CO, especially in layer 4. Such areas are likely to have a well-developed layer 4 of granule cells that is densely myelinated. In brain sections cut parallel to the brain surface, several of the histological preparations revealed a patchy pattern in some areas of cortex, suggesting that these areas have a modular organization.

Here, we discuss our results and conclusions for each major cortical region of the tree shrews in the context of previous architectonic and experimental studies of cortical organization in tree shrews, and, to a limited extent, in other mammals.

Occipital Cortex

The occipital cortex of tree shrews includes two architectonically distinct fields, areas 17 and 18, which correspond to visual areas V1 and V2 of other mammals. Areas lateral to area 18 include visual areas TA, TP, and TD, which also may be considered as parts of occipital cortex, but they are discussed here as parts of dorsal temporal cortex.

Area 17 has such pronounced sensory features that it was easily identified as such in early architectonic studies (Le Gros Clark, 1924; von Bonin and Bailey, 1961). These and a number of subsequent investigators (see Lund et al., 1985) were impressed with the very distinct layer 4 of granule cells, which is divided by a narrow, cell poor cleft into inner and outer halves (Figs. 1, 2), now identified as sublayers 4a and 4b (Lund et al., 1985). Both Le Gros Clark (1924) and von Bonin and Bailey (1961) considered the possibility that the 4a and 4b divisions of layer 4 in tree shrews are homologous to the outer and inner sublayers of layer 4 of primates (sublayers 4Cα and 4Cβ of Brodmann's (1909) terminology), as they considered tree shrews to be primates. We now know that 4a and 4b in tree shrews do not correspond to 4Cα and 4Cβ sublayers of primates, and they represent different evolutionary specializations of layer 4. In primates, layer 4Cα receives inputs from the magnocellular layers of the lateral geniculate nucleus, whereas layer 4Cβ receives inputs from the parvocellular layers (Casagrande and Kaas, 1994). In tree shrews, sublayers 4a and 4b each receive inputs from a mixture of lateral geniculate layers (Conley et al., 1984), and neurons in sublayer 4a are distinguished by responding to the onset of light, whereas neurons in 4b responded to the offset of light (Norton et al., 1985; Kretz et al., 1986). Sublayers of layer 4 are also apparent in CO preparations, with the middle portion of layer 4 expressing less CO (Fig. 1; also see Lund et al., 1985). In our preparations, layer 4 of tree shrews is also characterized by dense expressions of PV and VGluT2, reflecting dense inputs from the lateral geniculate nucleus of the sensory thalamus (Diamond et al., 1970; Harting et al., 1973). The very poor zinc staining of layer 4 indicates that this layer is dominated by thalamic rather than cortical inputs. Additionally, layer 4 of tree shrews, as well as cats and monkeys, expresses very little of the antigen for the Cat-301 antibody (Jain et al., 1994).

Layer 3 of tree shrews also has sublayers, with a cell sparse inner subdivision of layer 3, which is most obvious in Nissl preparations (Fig. 3A). Le Gros Clark (1924) speculated that this inner portion of layer 3 might correspond to a fiber dense band, the stria of Gennari, and our brain sections stained for myelin clearly indicate that the outer band of Baillarger, or the stria of Gennari, is in the inner portion of layer 3 that is sublayer 3c (also see Rockland et al., 1982). This result is in conflict with most current interpretations of layers 3 and 4 in primates, which place the stria of Gennari in sublayer 4B of Brodmann (1909). Thus, these results add to previous evidence that the laminar pattern of area 17 of monkeys has been misinterpreted, and that Brodmann's layer 4B of monkeys corresponds to layer 3C of tree shrews, galagos, and other mammals (for review, see Casagrande and Kaas, 1994). Note that sublayer 3b of tree shrews and cats expresses more of the antigen for Cat 301 than adjoining layers, as does the sublayer typically defined as layer 4B of macaques (Jain et al., 1994).

In addition to sublayer 3c, sublayers 3a and 3b have been distinguished in Nissl material from area 17 of tree shrews (e.g., Lund et al., 1985; Wong-Riley and Norton, 1988; Jain et al., 1994). Layer 3b is somewhat more densely packed with cells than sublayers 3c and 3a. In this study, we also found that sublayer 3b is distinguished from sublayers 3a and 3c by a patchy pattern of zinc poor regions and a dense expression of VGluT2 (Fig. 3). Both of these features suggest the existence of more inputs from the thalamus in layer 3b than in adjoining sublayers, and likely some input from the lateral geniculate nucleus, and such inputs from the lateral geniculate nucleus to layer 3b have been demonstrated (Hubel, 1975; Conley et al., 1984; Usrey et al., 1992). Our material also indicates that sublayer 3a expresses less PV and much more CB than sublayer 3b (Fig. 3). Finally, we were able to divide layer 5 into two distinct sublayers, 5a as a band of SMI-32-immunoreactive pyramidal cells and 5b with a dense expression of synaptic zinc (Fig. 3). As sublayer 3a also has considerable synaptic zinc, sublayers 3a and 5b are likely dominated by cortical inputs, perhaps those intrinsic to area 17.

We also observed architectonic features of area 17 in brain sections cut parallel to the artificially flattened cortex. In layer 3, an uneven distribution of myelin-light patches was surrounded by myelin-dark regions (Fig. 4), as previously reported by Lyon et al., (1998). In addition, synaptic zinc and VGluT2 were distributed in a patchy formation that was also apparent in layer 3b of transverse brain sections (Fig. 3). This modular pattern within area 17 of tree shrews is reminiscent of the CO-dark blobs of area 17 of primates, although tree shrews do not have CO blobs (e.g., Wong-Riley and Norton, 1988). However, the patchy pattern may reflect a pattern of VGluT2-rich terminals of the lateral geniculate nucleus inputs that are surrounded by walls of zinc-enriched terminals of intrinsic connections (Rockland et al., 1982; Sesma et al., 1984; Bosking et al., 1997). The CO blobs of primates receive inputs from the koniocellular layers of the lateral geniculate nucleus (see Casagrande and Kaas, 1994).

Area 18 of this study corresponds to the area 18 that was shown to be coextensive with the second visual

area, V2 by Kaas et al., (1972), a visual area common to nearly all mammals (Rosa and Krubitzer, 1999). In Nissl preparations, area 18 of tree shrews has less dense cell packing in layers 4 and 6 than in area 17 and in areas along the lateral border of area 18, such that the overall laminar pattern of area 18 is less distinct. Surprisingly, area 18 was not recognized by Le Gros Clark (1924), who divided cortex lateral to area 17 into a large parietal area, of which includes several of our subdivisions of cortex. Likewise, von Bonin and Bailey (1961) did not subdivide cortex lateral to V1. More recently, Zilles (1978) defined an area Oc2 as equivalent to area 18 and V2 in tree shrews. Oc2 of Zilles (1978) closely corresponds to area 18 of this study. Here, we show that area 18 expresses less PV and VGluT2 in axonal terminations, and more synaptic zinc in layer 4 and 6 than area 17. These observations are consistent with the evidence that area 18 receives more cortical inputs, including dense, topographically organized inputs from area 17 (Sesma et al., 1984; Lyon et al., 1998). The distributions of myelinated fibers in area 18 do not form distinct outer and inner bands of Baillarger, as in area 17, and in surface view preparations, area 18 appears to have an alternating pattern of myelin-light and myelin-dense bands or ovals. Cusick et al. (1985) found that the myelin-dense ovals corresponded to locations with dense clusters of callosally projecting neurons and callosal terminations. Thus, there is evidence for a modular organization in area 18 of tree shrews. Squirrels also have a similar pattern of myelin-dense and myelin-light modules in area 18 (Kaas et al., 1989), and monkeys have a modular pattern of myelin-dense and myelin-light bands in area 18 (e.g., Tootell et al., 1983; Cusik and Kaas, 1988; Krubitzer and Kaas, 1989). Area 18 of tree shrews is also distinguished by a greater expression of the antigen for Cat-301 in layer 3 than in adjoining cortex (Jain et al., 1994), and lower levels of CO in layer 4 than area 17 (Jain et al., 1994; this study). Thus, area 18 of tree shrews can be identified in a number of preparations.

Temporal Visual Cortex

In this study, we have retained the three divisions of temporal cortex along the outer border of V2 that were described as differing in V1 projections by Sesma et al (1984). In brief, a temporal dorsal (TD) area receives dense projections from V1; a more posterior region, the temporal posterior (TP) area receives a second pattern of dense projections from V1; whereas a more anterior region, the temporal anterior (TA) area receives only sparse inputs from V1. All three areas have connections with V2, and with each other, but only sparse connections with more ventral portions of the temporal lobe (Lyon et al., 1998). Other visual inputs come from the visual pulvinar (Lyon et al., 2003). Area TA and TD project to the forelimb portion of primary motor cortex (Remple et al., 2007), and thus can be considered visuomotor in function. Neurons in the region of TD were found to be responsive to visual stimuli, although the receptive fields were large and difficult to delineate (Kaufman and Somjen, 1979). Lesions of temporal cortex including much of TP, TD, and ITc regions produce impairments in visual learning (Killackey et al., 1971).

The architectonic borders of TA, TP, and TD are subtle. Previous studies have shown that TD is more densely myelinated than TA and TP (Sesma et al., 1984; Lyon et al., 1998), and that TA and TD express higher levels of the antigen for the Cat-301 antibody than TP (Jain et al., 1994). Higher levels of Cat-301 staining have been associated with structures having larger neurons with thicker, more rapidly conducting axons (e.g., Hockfield et al., 1983; Hendry et al., 1984)), whereas sensory areas are typically more densely myelinated than other fields (e.g., Hopf, 1964). Our results also show that TD is more densely myelinated than TA and TP. In addition, TD has a more developed, thicker layer 4 than TA and TP, as well as more VGluT2- and PV-immunopositive terminations, indicating the presence of thalamic inputs, and more synaptic zinc, indicating the presence of cortical terminations. The relative position of TD across from central V2 and V1, the dense inputs from both of these areas, together with pulvinar inputs and dense myelination, have lead to the hypothesis that TD is a homologue of primate area MT (Sesma et al., 1984; Kaas and Preuss, 1993; Jain et al., 1994; Northcutt and Kaas, 1995). If so, MT may have originated as a visual area adjacent to V2 (area 18), with the DL-V4 complex emerging later in evolution.

Inferior Temporal Cortex

We have included in the IT region of tree shrew cortex, areas ITc, ITi, and ITr, located in a caudodorsal to rostroventral sequence. We also include the temporal inferior area, TI, of Lyon et al. (1998) because of its position, and because TI, together with other divisions of IT cortex, receives inputs from a posterior division of the visual pulvinar, PP (Lyon et al., 2003). Although visual functions of IT cortex have not been physiologically demonstrated, connections with the visual pulvinar, and at least a few connections with cortical visual areas (Lyon et al., 1998), suggest that the IT areas of tree shrews are higher order visual or multisensory areas, as they are in other mammals (Wong et al., 2008). Large lesions that include the IT region are followed by impairments in visual behavior (Killackey et al., 1971).

TI was previously described as being more myelinated than surrounding cortex (Lyon et al., 1998). We found that TI expresses lower levels of zinc and higher levels of CO than surrounding cortex, perhaps as a result of inputs from the pulvinar (Lyon et al., 2003). Of the three other IT areas, ITi has the most features of a sensory area with thalamic input, including a well-developed layer 4, higher myelination, low levels of synaptic zinc, more CO expression, and more PV- and VGluT2-immunopositive terminations. ITi (TPI of Lyon et al., 1998) has more visual input from the TD-TP region of Lyon et al. (1998), as well as from two nuclei of the visual pulvinar with superior colliculus inputs (Lyon et al., 2003). Thus, ITi is likely to have visual functions. In contrast, ITr and ITc do not have architectonic features of a core sensory area, but rather the appearance of an association or higher order processing area. Thus, ITr and ITc have low myelination, a high expression of synaptic zinc, and low levels of PV and VGluT2 staining. ITr may be involved in auditory functions, as ITr is in the region identified as nonprimary auditory cortex by Oliver and Hall (1978) based on connections with the dorsal division

of the medial geniculate complex and the suprageniculate, as well as the visual pulvinar. There also appears to be some connections with motor cortex (Remple et al., 2007). Overall, the relative position, architectonic features, and cortical and subcortical connections of ITr of tree shrews are reminiscent of the temporal intermediate area of squirrels (Wong and Kaas, 2008; Wong et al., 2008). By position next to higher order visual areas TP and TD, ITc is likely to have visual functions.

Auditory Cortex

The auditory cortex of tree shrews contains at least one core sensory area and a surrounding belt region (Oliver and Hall, 1975; Casseday et al., 1976; Oliver and Hall, 1978). The core region (Ac) can be identified by being the target of topographically organized projections from the ventral subdivision of the medial geniculate nucleus, in addition to diffuse projections from the posterior nucleus and the medial (magnocellular) subdivision of the medial geniculate nucleus (Oliver and Hall, 1975; Casseday et al., 1976; Oliver and Hall, 1978). The surrounding Ab region receives inputs from the other subdivisions of the medial geniculate nucleus, such as the medial (magnocellular) and dorsal subdivision (Oliver and Hall, 1975; Casseday et al., 1976; Oliver and Hall, 1978) and the posterior nucleus (Diamond et al., 1970; Harting et al., 1973), and is differentiated from the core by the lack of inputs from the ventral subdivision of the medial geniculate (Oliver and Hall, 1975; Casseday et al., 1976; Oliver and Hall, 1978). Both Ac and Ab have a koniocellular appearance, such as a darkly stained granular layer 4 in Nissl preparations and dense myelination (Diamond et al., 1970; Oliver and Hall, 1975; Casseday et al., 1976; Oliver and Hall, 1978), and can be differentiated cytoarchitectonically by the thinner layer 4 and a less densely packed layer 3 in Ab (Oliver and Hall, 1978). These findings are congruent with our results. Both Ac and Ab are poorly populated by zinc-enriched terminals. In addition, layer 4 of Ac stains more intensely than layer 4 of Ab in VGluT2 and PV preparations, as expected of primary sensory cortex.

Parietal Cortex

Tree shrews have as many as eight parietal cortical areas; 3b(S1), the secondary somatosensory area (S2) and Pv area, the transitional area 3a, the SC area, and the PPd, PPr, and PPc areas. Of these eight areas, area 3b(S1) is the largest and has a topographic representation of the contralateral body surface (Lende, 1970; Sur et al., 1980, 1981a,b). The somatotopic organization of the contralateral body surface begins with the head representation laterally, proceeding to the hand, arm, rostral trunk, and over the medial wall to the tail, caudal trunk, and foot in a lateromedial progression (Lende, 1970; Sur et al., 1980, 1981b). This topographic pattern is similar to the 3b(S1)s of other mammals (for review, see Kaas, 1983). As expected of primary sensory areas, area 3b(S1) has a koniocellular appearance with a layer 4 that is densely packed with granule cells, expresses low levels of free zinc ions, and is densely packed with VGluT2- and PV-immunopositive thalamocortical terminals. This suggests that layer 4 receives proportionately more inputs from the thalamus than from other cortical areas. As with primary somatosensory cortex of other mammals, area 3b(S1) in tree shrews receives input from the ventroposterior nucleus (Diamond et al., 1970; Garraghty et al., 1991). As has been reported in other studies, the architectonic features of area 3b(S1) are not uniform throughout (Sur et al., 1980, 1981b; Cusick et al., 1985). In particular, the lateral part of area 3b(S1), where the face representation is located, has a thicker layer 4 (Sur et al., 1980). The nonuniform staining of 3b(S1) is also observed in sections stained for free zinc ions, VGluT2 and myelin. In favorable sections, the myelinated bands of Baillarger are discontinuous, which may be related to the discontinuities in the cortical representations of body parts, including the septa that invaginate 3b(S1), where the neurons have high response thresholds (Sur et al., 1980; Cusick et al., 1985).

Area 3b(S1) is bordered rostrally by area 3a, a narrow band of cortex where neurons are activated by taps to the body and noncutaneous stimuli (Sur et al., 1980; Kaas, 1983; Chapin and Lin, 1984). Area 3a receives topographically organized projections from area 3b(S1) and primary motor cortex (M1) (Remple et al., 2007). Area 3a is distinguished from area 3b(S1) by a reduction in thickness of layer 4, larger pyramidal cells in layer 5, reduction in myelination, increased expression levels of free zinc ions, and reduction in VGluT2 and PV staining. From the relative position and architectonic characteristics, area 3a in tree shrews is likely to be homologous to the intermediate sensorimotor area of Sanides and Krishnamurti (1967), postcentralis 2 region of Zilles (1978), and area 3a of rodents such as gray squirrels (Gould et al., 1989; Wong and Kaas, 2008) and primates (for review, Sur et al., 1980; see Slutsky et al., 2000 and Krubitzer et al., 2004).

The cortical area caudal to area 3b(S1), the caudal somatosensory area SC, was previously identified as the posterior somatic field (Sur et al., 1980). SC is characterized by a moderately populated layer 4, larger pyramidal cells in layer 5 in comparison to 3b(S1), and a reduced myelination level with no distinct bands of Baillarger. In layer 4, SC has higher expression levels of free zinc ions and lower expression of VGluT2- and PV-immunopositive thalamocortical terminations compared with 3b(S1), suggesting an increase in proportion of corticocortical over thalamocortical inputs. Area SC is responsive to more intense somatic stimuli (Sur et al., 1980) and has a rudimentary somatotopic map of the contralateral body (Remple et al., 2006, 2007). SC has dense, topographic connections with other somatosensory areas, such as 3a, 3b(S1), S2, and PV, and projections to motor cortex (Remple et al., 2007), as does the parietal medial area of squirrels (Krubitzer et al., 1986; Slutsky et al., 2000; Wong and Kaas, 2008) and rats (Donoghue and Parham, 1983; Reep et al., 1990, 1994; Wang and Kurata, 1998). It is also probable that SC of tree shrews is related to area 1/2 of galagos (Wu and Kaas, 2003) and area 1 of New World monkeys (Remple et al., 2007).

Areas S2 and Pv lie caudal and ventral to area 3b(S1). This region of cortex was previously considered to be a single, larger area that extends down into the rhinal fissure (Lende, 1970). Remple et al. (2006) established that S2 and Pv correspond to two separate, mirror image representations of the contralateral body surface, as with other mammals. Pv was also distinguished from S2 by a thinner and more densely packed layer 5 in Nissl

preparations. In the histochemical and immunohistochemical stains used here, S2 and Pv have similar architectonic characteristics, and as such, we did not define an architectonic border between the two areas. S2 and Pv are distinguished by the presence of a well-developed layer 4 that is thinner than that of 3b(S1) and higher levels of myelination than the dorsally adjoining SC. Layer 4 of S2 and PV expresses higher levels of free zinc ions and lower levels of VGluT2- and PV-immunopositive terminations. This suggests an increased proportion of corticocortical inputs over thalamocortical inputs, presumably because of the dense, somatopically organized inputs from 3b(S1) (Sur et al., 1981a; Weller et al., 1987). The somatotopic organizations of S2 and Pv in tree shrews are similar to those in squirrels (Nelson et al., 1979; Krubitzer et al., 1986) and rats (Walker and Sinha, 1972; Remple et al., 2003). Additionally, the architectonic characteristics of S2 and Pv in tree shrews are similar to those of gray squirrels (Krubitzer et al., 1986; Wong and Kaas, 2008).

The PP cortex of tree shrews is subdivided into three cortical areas, the PPr, equivalent to the posterior Pv area of Remple et al (2007), the PPc area, and the PPd area. PPc has the architectonic characteristics of an association cortex, with a thin layer 4 populated by small granule cells, lower myelination levels compared with the surrounding cortical areas and lower expression of CO. In zinc preparations, layer 4 of PPc expresses higher levels of free zinc ions compared with TI, and in VGluT2 and PV preparations, layer 4 of PPc expresses low levels of VGluT2- and PV-immunopositive terminations. This suggests a dominance of corticocortical inputs into layer 4 of PPc. PPc is likely to have a role in visuomotor processing, as it is interconnected with visual areas including area 18, TD, TP, and TA (Lyon et al., 1998) and projects to the M2 (Remple et al., 2007). The visual and premotor connections of PPc in tree shrews are similar to that of PP cortex in primates, suggesting some homology between the two regions.

The architectonic differences between PPr and PPd were not distinct, and an architectonic border between these two cortical fields was not reliably delimited. PPr and PPd are likely to be involved in the integration of visual and somatosensory information as they receive projections from visual areas, including area 18 and TA, and somatosensory areas, such as 3b(S1), S2, and Pv (Remple et al., 2007). This is reflected in the architectonic appearance of PPr and PPd as they show the characteristics of higher order, association areas, such as the absence of a well-developed granular layer 4 and lower myelination levels. Additionally, layer 4 of PPr and PPd is densely populated with zinc-enriched terminals and sparsely populated with VGluT2- and PV-immunopositive thalamocortical terminals, which suggests the presence of a larger proportion of corticocortical inputs. PPr and PPd can be teased apart by their connection patterns, as PPr projects topographically to the M1 (Remple et al., 2007).

Frontal Cortex

In frontal cortex of tree shrews, we have identified a primary motor cortex, M1, that has the general architectonic features of motor cortices, such as a poorly developed layer 4, a layer 5 that is populated with large SMI-32-immunopositive pyramidal cells, and poor myelination. This architectonically defined field corresponds to the electrophysiologically defined primary motor cortex that has a topographic arrangement of contralateral body movements (Remple et al., 2006). Layer 4 of M1 stains darkly in zinc preparations and poorly for VGluT2- and PV-immunopositive terminations, similar to the agranular motor cortex in gray squirrels (Wong and Kaas, 2008). This suggests that larger proportion of inputs into layer 4 of M1 originates from other cortical areas rather than from thalamic nuclei. Anatomical tracing studies have shown that M1 has dense connections with M2, which is rostral to M1, and receives inputs somatosensory areas such as 3b(S1), the PP cortex, and temporal visual areas such as TA and TD (Remple et al., 2007). Neurons in M2 have a higher current threshold than those in M1 (Remple et al., 2006). Architectonically, M2 is differentiated from M1 by a less densely packed layer 5 with smaller sized SMI-32-immunopositive pyramidal cells in layer 5. The general connectivity pattern of M2 is similar to M1. Differences include denser projections from PPc and ITr (TIV) to M2 than to M1 (Remple et al., 2007).

The combined extent of both M1 and M2 is comparable to the praecentralis 1 region that was distinguished in tree shrew by Zilles (1978). M1 of tree shrews has similar neuron response properties, organization, and architectonic characteristics of primary motor cortex of other mammals, such as the lateral agranular cortex of rats (Donoghue and Wise, 1982; Neafsey et al., 1986; Wise and Donoghue, 1986; Brecht et al., 2004). The organizations, architectures, and locations of M1 and M2 in tree shrews bear some similarity to the motor and premotor areas in prosimians and primates (Wise, 1985; Matelli et al., 1986; Barbas and Pandya, 1987; Stepniewska et al., 1993; Wu et al., 2000; Fang et al., 2005). As such, it has been proposed that M2 of tree shrews may be homologous to the premotor cortex of primates (Remple et al., 2006).

We have divided the frontal pole of tree shrews into two main architectonically distinct cortical regions, the DFC and the OFC, much like the division of the frontal pole in rats and rabbits into the medial and lateral frontal polar areas (Ray and Price, 1992; Uylings et al., 2003; Gabbott et al., 2005; Leal-Campanario et al., 2007). However, the frontal areas of tree shrews have a distinct granular layer, and as such, have a closer resemblance to the frontal polar region of squirrels (Wong and Kaas, 2008), and the prefrontal cortex of galagos (Preuss and Goldman-Rakic, 1989, 1991) and other primates (Preuss et al., 1997), than the agranular prefrontal cortex of rats (Öngür and Price, 2000). In addition, layer 4 of OFC, and to a lesser extent of DFC, has a lower expression of zinc-enriched corticocortical terminations and a higher expression of VGluT2- and PV-immunopositive thalamocortical terminations, which suggests the present of a dominant population of thalamocortical inputs into the area. In galagos, the lateral frontal lobe and orbital prefrontal cortex receives inputs from the mediodorsal nucleus of the thalamus, and the posterolateral cortex receives inputs from the ventral thalamic complex (Markowitsch et al., 1980). However, the frontal polar region of tree shrews is not as complex as that of galagos (Preuss and Goldman-Rakic, 1989, 1991) and other primates (Preuss et al, 1997). Both DFC and OFC

of tree shrews have a sparse to almost absent population of SMI-32-immunopositive pyramidal cells, whereas layer 3 of granular prefrontal cortex of galagos and macaques is populated by a specialized type of spinous pyramidal cells that have been suggested to play a role in the evolution of intellectual complexity in primates (Elston et al., 2005). The frontal polar region of tree shrews may have a more complex organization complex than the scheme proposed here, and may be subdivided into more cortical areas, as we have not attempted to make fine architectonic distinctions. Studies of cortical connections might be useful in further subdividing the region.

Medial Cortex

The MF area of tree shrews approximately corresponds to area praecentralis 3 of Zilles (1978). MF has a well-developed layer 4 and a sparsely populated layer 5, and bears an architectonic resemblance to the pre-SMA region in galagos (Wu et al., 2000) that has been identified as the granular medial and MF region of galagos by Preuss and Goldman-Rakic (1991) and area F6 of monkeys (Matelli et al., 1991). MF is also in the approximate location of the frontal and rostral cingulate area of gray squirrels, but unlike MF, the rostral cingulate region of gray squirrels does not have a well-developed layer 4 and is poorly myelinated (Wong and Kaas, 2008). MF expresses moderate levels of free zinc ions and has a sparse distribution of VGluT2- and PV-immunopositive terminations, indicating that there is a dominance of corticocortical inputs over thalamocortical inputs. Studies of connections would be needed to confirm this deduction.

The MMA adjoins M1 along the medial wall and was identified as a region that has dense, topographically organized projections to M1 and M2 (Remple et al., 2007). MMA is likely to have representations of the face and forelimb, although there has been little success in eliciting movements from MMA in microstimulation studies (Remple et al., 2006, 2007). Architectonically, MMA shares some characteristics with M1, such as a poorly developed layer 4, a thick layer 5 that is densely populated with pyramidal cells, and similar myelination levels. MMA expresses high levels of zinc-enriched terminals and low levels of VGluT2- and PV-immunopositive thalamocortical terminals. This suggests that MMA receives stronger inputs from other cortical areas compared with thalamic nuclei.

Cingulate cortex of tree shrews is subdivided into the CGd, CGv, infraradiata dorsal (IRd), and infradiata ventral (IRv) areas. Various nomenclatures have been used for the cingulate cortical areas, depending on investigator and the species studied. For example, in rats, the anterior cingulate dorsal area of Jones et al. (2005) corresponds to area 24 and part of 32 of Kreig (1946), 24b and 24b′ of Vogt and Peters (1981) and Cg1 of Zilles and Wree (1995), and is homologous to area 24 of Brodmann (1909) and IRcα and IRbα of Rose (1931) in rabbits (see Jones et al., 2005; Zilles, 2004 for review). In this study, we partly use the nomenclature used by Zilles (1978) for tree shrews. CGd and CGv correspond to the anterior cingularis ventralis of Zilles (1978), and IRd and IRv were retained from Zilles (1978).

CGd does not have a well-developed layer 4 and is distinguished from CGv as CGd has a higher cell packing density and a more homogenous appearance. The architectonic appearance of CGv varies along its dorsoventral extent, especially in the Nissl and zinc preparations, suggesting the possibility for further subdivisions. Both CGv and CGd have reduced staining of VGluT2- and PV-immunopositive terminations in layer 4, indicating that these areas receive proportionately less thalamocortical input than adjacent cortical areas such as area 3b(S1). Unlike in rats (Zilles, 1990; Jones et al., 2005) and squirrels (Wong and Kaas, 2008), where the cingulate regions occupy the dorsal extent of the rostral medial wall, the frontal cingulate areas in tree shrews are displaced ventrally by the somatosensory areas, 3a, 3b(S1), and SC, much as in primates (e.g., Wu and Kaas, 2003).

IRd shares some architectonic features of the cingulate cortex in rats (Zilles, 1990; Vogt et al., 2004), such as the poorly developed layer 4 and moderate myelination. In rats, the cingulate cortex receives diffuse projections from the mediodorsal, ventromedial, and anteromedial nuclei of the thalamus (Domesick, 1969) and has extensive connections with various cortical areas, including the visual and motor cortex (Vogt and Miller, 1983). In tree shrews, IRd expresses high levels of zinc-enriched terminals and low levels of VGluT2- and PV-immunopositive terminals, indicating that inputs into IRd originate predominantly in other cortical areas.

IRv is in the approximate location of the medial somatosensory area (MSA) of Remple et al. (2007). Neurons in MSA have larger receptive fields than neurons in 3b(S1) and MSA sends dense projections to both M1 and M2 (Remple et al., 2007). Architectonically, IRv has a thin layer 4 and is less heavily myelinated than IRd, with a thin, distinct outer band of Baillarger. IRv expresses high levels of zinc-enriched terminals and moderate levels of VGluT2- and PV-immunopositive terminals, indicating that inputs into IRv originate from the thalamus, as well as other cortical areas.

Area PS is a limbic area that was identified in primates by Sanides (1970) and is visual in function, representing the peripheral vision of the contralateral visual hemifield. This area has been identified in cats as the splenial visual area (see Rosa and Krubitzer, 1999 for review), and is comparable to the posteromedial visual area in rats and mice (Wang and Burkhalter, 2007), medial area 18b (Krieg, 1946; Caviness, 1975), and Oc2MM (Zilles and Wree, 1995). In tree shrews, PS has a poorly developed layer 4, does not have a well-defined laminar pattern, and is poorly myelinated, similar to the PS of primates (Allman and Kaas, 1971) and gray squirrels (Wong and Kaas, 2008). Area PS is likely to have a larger proportion of corticocortical, rather than thalamocortical, inputs, as it expressed high levels of free zinc ions and a near absence of VGluT2- and PV-immunopositive terminations.

The retrosplenial cortex has been subdivided in to granular (RSg) and agranular areas (RSag) in a previous study by Zilles (1978). Both RSg and RSag do not have well-defined laminar patterns. RSg is characterized by a densely populated layer 2/3 and is moderately myelinated, whereas RSag has a low cell packing density and is lightly myelinated. Layer 2/3 of RSag expresses higher levels of zinc-enriched corticocortical terminations and lower levels of VGluT2- and PV-immunopositive

thalamocortical terminations compared with RSg. This suggests that a higher proportion of the inputs into layer 2/3 of RSag originate from other cortical areas, whereas a high proportion of inputs into layer 2/3 of RSg originate from nuclei in the thalamus.

Remaining Cortical Areas

The insular cortex (Ins) defined here is distinctly laminated and has a well-developed granular layer 4. The low expression of zinc-enriched corticortical terminations in layer 4 of Ins suggests that this layer has few corticortical inputs. Layer 4 of Ins expresses high levels of VGluT2- and PV-immunopositive terminations, indicating the presence of dense inputs from the thalamus. In primates, the granular posterior portion of the insular has a dense population of thalamocortical terminations (Jones and Burton, 1976). Anatomical tract tracing studies in primates have shown that Ins has dense connections with the auditory cortex, temporal cortex, and the parvocellular subdivision of the medial geniculate nucleus (Augustine, 1985; Mesulam and Mufson, 1985). In addition, electrophysiological studies have shown the presence of auditory responsive units in the insular (Sudakov et al., 1971). Ins of tree shrews approximately corresponds in location to the parietal insular cortex of rats (Shi and Cassell, 1998), as both regions lie ventral to 3b(S1) and S2. In rats, the granular zone of insular cortex is involved in viscerosensory modalities (Kosar et al., 1986; Cechetto and Saper, 1987; Sewards and Sewards, 2001). Similar to the posterior insular cortex in primates, part of the granular insular zone of rats receives strong inputs from S2 (Shi and Cassell, 1997), as well as from 3b(S1) and the posterior thalamic nucleus (Shi and Cassell, 1998). Much of this somatosensory zone of granular insular cortex is in the region of somatosensory area Pv as defined by Remple et al. (2003) in rats, and this would correspond to the Pv area of tree shrews rather than the insular cortex.

Perirhinal area (PRh) is retained from Zilles and Wree (1985) and corresponds to areas 35 and 36 of Brodmann (1909), the posterior region of area 35 of Krieg (1946), and the ectorhinal and PRhs of Swanson (2003). As with other mammals, such as gray squirrels (Wong and Kaas, 2008), and rats (Burwell, 2001; Palomero-Gallagher and Zilles, 2004), PRh is poorly myelinated and has a poorly defined lamination pattern. The dark staining in zinc preparations suggests that a large proportion of inputs to PRh is from other areas of cortex. PRh has been suggested to have a role in memory processes, as it has connections with the hippocampal formation (Burwell and Amaral, 1998; Palomero-Gallagher and Zilles, 2004; Furtak et al., 2007). In addition, PRh in rats has connections with the anterior thalamic nuclei (Palomero-Gallagher and Zilles, 2004), and the piriform, frontal, temporal, and insular cortical areas (Furtak et al., 2007).

ACKNOWLEDGMENTS

The authors thank Laura Trice for help with the histological procedures. Dr. David Fitzpatrick kindly provided the tree shrews for this study.

LITERATURE CITED

Abplanalp P. 1970. Some subcortical connections of the visual system in tree shrews and squirrels. Brain Behav Evol 3:155–168.

Allman JM, Kaas JH. 1971. Representation of the visual field in striate and adjoining cortex of the owl monkey (*Aotus trivirgatus*). Brain Res 35:89–106.

Augustine JR. 1985. The insular lobe in primates including humans. Neurol Res 7:2–10.

Barbas H, Pandya DN. 1987. Architecture and frontal cortical connections of the premotor cortex (area 6) in the rhesus monkey. J Comp Neurol 256:211–228.

Bishop A. 1964.Use of the hand in lower primates. In: Buettner-Janusch J, editor. Evolutionary and genetic biology of primates. New York: Academic Press. p 133–225.

Bosking WH, Zhang Y, Schofield B, Fitzpatrick D. 1997. Orientation selectivity and the arrangement of horizontal connections in tree shrew striate cortex. J Neurosci 17:2112–2127.

Brecht M, Krauss A, Muhammad S, Sinai-Esfahani L, Bellanca S, Margrie TW. 2004. Organization of rat vibrissa motor cortex and adjacent areas according to cytoarchitectonics, microstimulation, and intracellular stimulation of identified cells. J Comp Neurol 479:360–373.

Brodmann K. 1909. Brodmann's 'localisation in the cerebral cortex'. London: Eldred Smith-Gordon.

Burwell RD. 2001. Borders and cytoarchitecture of the perirhinal and postrhinal cortices in the rat. J Comp Neurol 437:17–41.

Burwell RD, Amaral DG. 1998. Cortical afferents of the perirhinal, postrhinal, and entorhinal cortices of the rat. J Comp Neurol 398: 179–205.

Campbell MJ, Morrison JH. 1989. Monoclonal antibody to neurofilament protein (SMI-32) labels a subpopulation of pyramidal neurons in the human and monkey neocortex. J Comp Neurol 282: 191–205.

Casagrande VA, Kaas JH. 1994. The afferent, intrinsic and efferent connections of primary visual cortex in primates. In: Peters A, Rockland KS, editors. Cerebral cortex. New York: Plenum Press. p 201–259.

Casseday HJ, Diamond IT, Harting JK. 1976. Auditory pathways to the cortex in *Tupaia glis*. J Comp Neurol 166:303–340.

Caviness VS, Jr. 1975. Architectonic map of neocortex of the normal mouse. J Comp Neurol 164:247–263.

Cechetto DF, Saper CB. 1987. Evidence for a viscerotopic sensory representation in the cortex and thalamus in the rat. J Comp Neurol 262:27–45.

Celio MR. 1986. Parvalbumin in most γ-aminobutyric acid-containing neurons of the rat cerebral cortex. Science 231:995–997.

Chapin JK, Lin CS. 1984. Mapping the body representation in the SI cortex of anesthetized and awake rats. J Comp Neurol 229: 199–213.

Conde F, Lund JS, Lewis DA. 1996. The hierarchical development of monkey visual cortical regions as revealed by the maturation of parvalbumin-immunoreactive neurons. Brain Res Dev Brain Res 96:261–276.

Conley M, Fitzpatrick D, Diamond IT. 1984. The laminar organization of the lateral geniculate body and the striate cortex in the tree shrew (*Tupaia glis*). J Neurosci 4:171–197.

Cruikshank SJ, Killackey HP, Metherate R. 2001. Parvalbumin and calbindin are differentially distributed within primary and secondary subregions of the mouse auditory forebrain. Neuroscience 105:553–569.

Cusik CG, Kaas JH. 1988. Cortical connections of area 18 and dorsolateral visual cortex in squirrel monkeys. Vis Neurosci 1: 211–237.

Cusick CG, MacAvoy MG, Kaas JH. 1985. Interhemispheric connections of cortical sensory areas in tree shrews. J Comp Neurol 235: 111–128.

Danscher G. 1981. Histochemical demonstration of heavy metals. A revised version of the sulphide silver method suitable for both light and electronmicroscopy. Histochemistry 71:1–16.

Danscher G. 1982. Exogenous selenium in the brain. A histochemical technique for light and electron microscopical localization of catalytic selenium bonds. Histochemistry 76:281–293.

Danscher G, Stoltenberg M. 2005. Zinc-specific autometallographic in vivo selenium methods: tracing of zinc-enriched (ZEN) terminals, ZEN pathways, and pools of zinc ions in a multitude of other ZEN cells. J Histochem Cytochem 53:141–153.

de Venecia RK, Smelser CB, McMullen NT. 1998. Parvalbumin is expressed in a reciprocal circuit linking the medial geniculate body and auditory neocortex in the rabbit. J Comp Neurol 400: 349–362.

DeFelipe J. 1997. Types of neurons, synaptic connections and chemical characteristics of cells immunoreactive for calbindin-D28K, parvalbumin and calretinin in the neocortex. J Chem Neuroanat 14:1–19.

DeFelipe J, Jones EG. 1991. Parvalbumin immunoreactivity reveals layer IV of monkey cerebral cortex as a mosaic of microzones of thalamic afferent terminations. Brain Res 562:39–47.

Diamond IT, Snyder M, Killackey H, Jane J, Hall WC. 1970. Thalamo-cortical projections in the tree shrew (*Tupaia glis*). J Comp Neurol 139:273–306.

Domesick VB. 1969. Projections from the cingulate cortex in the rat. Brain Res 12:296–320.

Donoghue JP, Parham C. 1983. Afferent connections of the lateral agranular field of the rat motor cortex. J Comp Neurol 217: 390–404.

Donoghue JP, Wise SP. 1982. The motor cortex of the rat: cytoarchitecture and microstimulation mapping. J Comp Neurol 212: 76–88.

Elston GN, Elston A, Casagrande V, Kaas JH. 2005. Areal specialization of pyramidal cell structure in the visual cortex of the tree shrew: a new twist revealed in the evolution of cortical circuitry. Exp Brain Res 163:13–20.

Emmons LH. 2000. Tupai: a field study of bornean tree shrews. Berkeley, CA: University of California Press.

Fang PC, Stepniewska I, Kaas JH. 2005. Ipsilateral cortical connections of motor, premotor, frontal eye, and posterior parietal fields in a prosimian primate, *Otolemur garnettii*. J Comp Neurol 490: 305–333.

Fitzpatrick D. 1996. The functional organization of local circuits in visual cortex: insights from the study of tree shrew striate cortex. Cereb Cortex 6:329–341.

Fujiyama F, Furuta T, Kaneko T. 2001. Immunocytochemical localization of candidates for vesicular glutamate transporters in the rat cerebral cortex. J Comp Neurol 435:379–387.

Furtak SC, Wei SM, Agster KL, Burwell RD. 2007. Functional neuroanatomy of the parahippocampal region in the rat: the perirhinal and postrhinal cortices. Hippocampus 17:709–722.

Gabbott PL, Warner TA, Jays PR, Salway P, Busby SJ. 2005. Prefrontal cortex in the rat: projections to subcortical autonomic, motor, and limbic centers. J Comp Neurol 492:145–177.

Gallyas F. 1979. Silver staining of myelin by means of physical development. Neurol Res 1:203–209.

Garraghty PE, Florence SL, Tenhula WN, Kaas JH. 1991. Parallel thalamic activation of the first and second somatosensory areas in prosimian primates and tree shrews. J Comp Neurol 311:289–299.

Gould HJ, III, Whitworth RHJ, LeDoux MS. 1989. Thalamic and extrathalamic connections of the dysgranular unresponsive zone in the grey squirrel (*Sciurus carolinensis*). J Comp Neurol 287: 38–63.

Hackett TA, Stepniewska I, Kaas JH. 1998. Subdivisions of auditory cortex and ipsilateral cortical connections of the parabelt auditory cortex in macaque monkeys. J Comp Neurol 394:475–495.

Harting JK, Diamond IT, Hall WC. 1973. Anterograde degeneration study of the cortical projections of the lateral geniculate and pulvinar nuclei in the tree shrew (*Tupaia glis*). J Comp Neurol 150: 393–440.

Hendry SH, Hockfield S, Jones EG, McKay R. 1984. Monoclonal antibody that identifies subsets of neurones in the central visual system of monkey and cat. Nature 307:267–269.

Hockfield S, McKay RD, Hendry SH, Jones EG. 1983. A surface antigen that identifies ocular dominance columns in the visual cortex and laminar features of the lateral geniculate nucleus. Cold Spring Harb Symp Quant Biol 48 (Part 2):877–889.

Hof PR, Glezer I, Conde F, Flagg RA, Rubin MB, Nimchinsky EA, Vogt Weisenhrn DM. 1999. Cellular distribution of the calcium-binding proteins parvalbumin, calbindin, and calretinin in the neocortex of mammals: phylogenetic and developmental patterns. J Chem Neuroanat 16:77–116.

Hopf A. 1964. Localisation in the cerebral cortex from the anatomical point of view. Madison: The University of Wisconsin Press. p 5–16.

Hubel DH. 1975. An autoradiographic study of the retino-cortical projections in the tree shrew (Tupaia glis). Brain Res 96:41–50.

Huchon D, Madsen O, Sibbald MJ, Ament K, Stanhope MJ, Catzeflis F, et al. 2002. Rodent phylogeny and a timescale for the evolution of glires: evidence from an extensive taxon sampling using three nuclear genes. Mol Biol Evol 19:1053–1065.

Humphrey AL, Norton TT. 1980. Topographic organization of the orientation column system in the striate cortex of the tree shrew (*Tupaia glis*). I. Microelectrode recording. J Comp Neurol 192: 531–547.

Ichinohe N, Rockland KS. 2004. Region specific micromodularity in the uppermost layers in primate cerebral cortex. Cereb Cortex 14: 1173–1184.

Jain N, Preuss TM, Kaas JH. 1994. Subdivisions of the visual system labeled with the cat-301 antibody in tree shrews. Vis Neurosci 11:731–741.

Jones BF, Groenewegen HJ, Witter MP. 2005. Intrinsic connections of the cingulate cortex in the rat suggest the existence of multiple functionally segregated networks. Neuroscience 133:193–207.

Kaas JH. 1983. What, if anything, is SI? Organization of first somatosensory area of cortex Physiol Rev 63:206–231.

Kaas JH, Catania KC. 2002. How do features of sensory representations develop? Bioessays 24:334–343.

Kaas JH, Krubitzer LA, Johanson KL. 1989. Cortical connections of areas 17 (V-I) and 18 (V-II) of squirrels. J Comp Neurol 281: 426–446.

Kaas JH, Hall WC, Killackey H, Diamond IT. 1972. Visual cortex of the tree shrew (*Tupaia glis*): architectonic subdivisions and representations of the visual field. Brain Res 42:491–496.

Kaas JH, Huerta MF. 1988. Subcortical visual system of primates. In: Steklis HD, Erwin J, editors. Comparative primate biology, Vol. 4: Neurosciences. New York: Alan Liss. p 327–391.

Kaas JH, Krubitzer LA, Johanson KL. 1989. Cortical connections of areas 17 (V-I(and 18 (V-II(of squirrels J Comp Neurol 281: 426–446.

Kaas JH, Preuss TM. 1993. Archontan affinities as refleted in the visual system. In: Szalay F, Novacek M, McKenna M, editors. Mammalian phylogeny. New York: Springer Verlag. p 115–128.

Kaneko T, Fujiyama F. 2002. Complementary distribution of vesicular glutamate transporters in the central nervous system. Neurosci Res 42:243–250.

Kaufman PG, Somjen GG. 1979. Receptive fields of neurons in area 17 and 18 of tree shrew (*Tupaia glis*). Brain Res Bull 4:319–325.

Killackey H, Snyder M, Diamond IT. 1971. Function of striate and temporal cortex in the tree shrew. J Comp Physiol Psychol 74 (Suppl 2):1–29.

Kosar E, Grill HJ, Norgren R. 1986. Gustatory cortex in the rat. I. Physiological properties and cytoarchitecture. Brain Res 379:329–341.

Kretz R, Rager G, Norton TT. 1986. Laminar organization of ON and OFF regions and ocular dominance in the striate cortex of the tree shrew (Tupaia belangeri). J Comp Neurol 251:135–145.

Krieg WJS. 1946. Connections of the cerebral cortex. I. The albino rat. A. Topography of the cortical areas. J Comp Neurol 84: 221–275.

Krubitzer LA, Kaas JH. 1989. Cortical integration of parallel pathways in the visual system of primates. Brain Res 478:161–165.

Krubitzer L, Huffman KJ, Disbrow E, Recanzone G. 2004. Organization of area 3a in macaque monkeys: contributions to the cortical phenotype. J Comp Neurol 471:97–111.

Krubitzer LA, Sesma MA, Kaas JH. 1986. Microelectrode maps, myeloarchitecture, and cortical connections of three

somatotopically organized representations of the body surface in the parietal cortex of squirrels. J Comp Neurol 250:403–430.
Lane RH, Allman JM, Kaas JH. 1971. Representation of the visual field in the superior colliculus of the grey squirrel (*Sciurus carolinensis*) and the tree shrew (*Tupaia glis*). Brain Res 26:277–292.
Latawiec D, Martin KA, Meskenaite V. 2000. Termination of the geniculocortical projection in the striate cortex of macaque monkey: a quantitative immunoelectron microscopic study. J Comp Neurol 419:306–319.
Le Gros Clark WE. 1924. On the brain of the tree-shrew (*Tupaia mior*). Proc Acad Soc (Lond) 77:1179–1309.
Le Gros Clark WE. 1959. The antecedents of man. Edinburgh: Edinburgh University Press.
Leal-Campanario R, Fairen A, Delgado-Garcia JM, Gruart A. 2007. Electrical stimulation of the rostral medial prefrontal cortex in rabbits inhibits the expression of conditioned eyelid responses but not their acquisition. Proc Natl Acad Sci USA 104:11459–11464.
Lee VM, Carden MJ, Schlaepfer WW, Trojanowski JQ. 1987. Monoclonal antibodies distinguish several differentially phosphorylated states of the two largest rat neurofilament subunits (NF-H and NF-M) and demonstrate their existence in the normal nervous system of adult rats. J Neurosci 7:3474–3488.
Lende RA. 1970. Cortical localization in the tree shrew (*Tupaia*). Brain Res 18:61–75.
Liu FG, Miyamoto MM, Freire NP, Ong PQ, Tennant MR, Young TS, et al. 2001. Molecular and morphological supertrees for eutherian (placental) mammals. Science 291:1786–1789.
Lund JS, Fitzpatrick D, Humphrey AL. 1985. The striate visual cortex of the tree shrew. In: Jones EG, Peters A, editors. Visual cortex. New York: Plenum Press. p 157–205.
Lyon DC, Jain N, Kaas JH. 1998. Cortical connections of striate and extrastriate visual areas in tree shrews. J Comp Neurol 401: 109–128.
Lyon DC, Jain N, Kaas JH. 2003. The visual pulvinar in tree shrews. II. Projections of four nuclei to areas of visual cortex. J Comp Neurol 467:607–627.
Markowitsch HJ, Pritzel M, Wilson M, Divac I. 1980. The prefrontal cortex of a prosimian (*Galago senegalensis*) defined as the cortical projection area of the thalamic mediodorsal nucleus. Neuroscience 5:1771–1779.
Matelli M, Camarda R, Glickstein M, Rizzolatti G. 1986. Afferent and efferent projections of the inferior area 6 in the macaque monkey. J Comp Neurol 251:281–298.
Matelli M, Luppino G, Rizzolatti G. 1991. Architecture of superior and mesial area 6 and the adjacent cingulate cortex in the macaque monkey. J Comp Neurol 311:445–462.
Mesulam MM, Mufson EJ. 1985. The insula of reil in man and monkey. Architectonics, connectivity and function. In: Jones EG, Peters A, editors. Cerebral cortex. New York: Plenum Press. p 179–226.
Murphy WJ, Eizirik E, Johnson WE, Zhang YP, Ryder OA, O'Brien SJ. 2001a. Molecular phylogenetics and the origins of placental mammals. Nature 409:614–618.
Murphy WJ, Eizirik E, O'Brien SJ, Madsen O, Scally M, Douady CJ, et al. 2001b. Resolution of the early placental mammal radiation using bayesian phylogenetics. Science 294:2348–2351.
Nahmani M, Erisir A. 2005. Vglut2 immunochemistry identifies thalamocortical terminals in layer 4 of adult and developing visual cortex. J Comp Neurol 484:458–473.
Neafsey EJ, Bold EL, Haas G, Hurley-Gius KM, Quirk G, Sievert CF, et al. 1986. The organization of the rat motor cortex: a microstimulation mapping study. Brain Res 396:77–96.
Nelson RJ, Sur M, Kaas JH. 1979. The organization of the second somatosensory area (smii) of the grey squirrel. J Comp Neurol 184:473–489.
Northcutt RG, Kaas JH. 1995. The emergence and evolution of mammalian neocortex. Trends Neurosci 18:373–379.
Norton TT, Rager G, Kretz R. 1985. ON and OFF regions in layer IV of striate cortex. Brain Res 327:319–323.
Oliver DL, Hall WC. 1975. Subdivisions of the medial geniculate body in the tree shrew (*Tupaia glis*). Brain Res 86:217–227.
Oliver DL, Hall WC. 1978. The medial geniculate body of the tree shrew, *Tupaia glis*. II. Connections with the neocortex. J Comp Neurol 182:459–493.
Ongur D, Price JL. 2000. The organization of networks within the orbital and medial prefrontal cortex of rats, monkeys and humans. Cereb Cortex 10:206–219.
Palomero-Gallagher N, Zilles K. 2004. Isocortex. In: Paxinos G, editor. The rat nervous system. London: Elsevier. p 729–757.
Preuss TM, Goldman-Rakic PS. 1989. Connections of the ventral granular frontal cortex of macaques with perisylvian premotor and somatosensory areas: anatomical evidence for somatic representation in primate frontal association cortex. J Comp Neurol 282:293–316.
Preuss TM, Goldman-Rakic PS. 1991. Architectonics of the parietal and temporal association cortex in the strepsirhine primate galago compared to the anthropoid primate macaca. J Comp Neurol 310:475–506.
Preuss TM, Stepniewska I, Jain N, Kaas JH. 1997. Multiple divisions of macaque precentral motor cortex identified with neurofilament antibody SMI-32. Brain Res 767:148–153.
Pritzel M, Kretz R, Rager G. 1988. Callosal projections between areas 17 in the adult tree shrew (*Tupaia belangeri*). Exp Brain Res 72:481–493.
Ray JP, Price JL. 1992. The organization of the thalamocortical connections of the mediodorsal thalamic nucleus in the rat, related to the ventral forebrain-prefrontal cortex topography. J Comp Neurol 323:167–197.
Reep RL, Chandler HC, King V, Corwin JV. 1994. Rat posterior parietal cortex: topography of corticocortical and thalamic connections. Exp Brain Res 100:67–84.
Reep RL, Goodwin GS, Corwin JV. 1990. Topographic organization in the corticocortical connections of medial agranular cortex in rats. J Comp Neurol 294:262–280.
Remple MS, Henry EC, Catania KC. 2003. Organization of somatosensory cortex in the laboratory rat (*Rattus norvegicus*): evidence for two lateral areas joined at the representation of the teeth. J Comp Neurol 467:105–118.
Remple MS, Reed JL, Stepniewska I, Kaas JH. 2006. Organization of frontoparietal cortex in the tree shrew (*Tupaia belangeri*). I. Architecture, microelectrode maps, and corticospinal connections. J Comp Neurol 497:133–154.
Remple MS, Reed JL, Stepniewska I, Lyon DC, Kaas JH. 2007. The organization of frontoparietal cortex in the tree shrew (*Tupaia belangeri*). II. Connectional evidence for a frontal-posterior parietal network. J Comp Neurol 501:121–149.
Rockland KS, Lund JS, Humphrey AL. 1982. Anatomical binding of intrinsic connections in striate cortex of tree shrews (*Tupaia glis*). J Comp Neurol 209:41–58.
Rosa MG, Krubitzer LA. 1999. The evolution of visual cortex: where is V2? Trends Neurosci 22:242–248.
Rose M. 1931. Cytoarchitektonischer atlas der grosshinrinde der maus. J Psychol Neurol 43:353–430.
Sanides F. 1970. Functional architecture of motor and sensory cortices in primates in the light of a new concept of neocortex evolution. In: Montagna W, editor. The primate brain. New York: Appleton-Century-Crofts. 137–208.
Sanides F, Krishnamurti A. 1967. Cytoarchitectonic subdivisions of sensorimotor and prefrontal regions and of bordering insular and limbic fields in slow loris (*Nycticebus coucang* coucang). J Hirnforsch 9:225–252.
Sesma MA, Casagrande VA, Kaas JH. 1984. Cortical connections of area 17 in tree shrews. J Comp Neurol 230:337–351.
Sewards TV, Sewards MA. 2001. Cortical association areas in the gustatory system. Neurosci Biobehav Rev 25:395–407.
Shi CJ, Cassell MD. 1997. Cortical, thalamic, and amygdaloid projections of rat temporal cortex. J Comp Neurol 382:153–175.
Shi CJ, Cassell MD. 1998. Cortical, thalamic, and amygdaloid connections of the anterior and posterior insular cortices. J Comp Neurol 399:440–468.
Slutsky DA, Manger PR, Krubitzer L. 2000. Multiple somatosensory areas in the anterior parietal cortex of the california ground squirrel (*Spermophilus beecheyii*). J Comp Neurol 416:521–539.

Sorenson M. 1970. Behaviour of tree shrews. Primate Behav 1: 141–193.

Springer MS, Murphy WJ, Eizirik E, O'Brien SJ. 2003. Placental mammal diversification and the cretaceous-tertiary boundary. Proc Natl Acad Sci USA 100:1056–1061.

Stepniewska I, Preuss TM, Kaas JH. 1993. Architectonics, somatotopic organization, and ipsilateral cortical connections of the primary motor area (M1) of owl monkeys. J Comp Neurol 330: 238–271.

Sudakov K, MacLean PD, Reeves A, Marino R. 1971. Unit study of exteroceptive inputs to claustrocortex in awake, sitting, squirrel monkey. Brain Res 28:19–34.

Sur M, Weller RE, Kaas JH. 1980. Representation of the body surface in somatosensory area I of tree shrews, *Tupaia glis*. J Comp Neurol 194:71–95.

Sur M, Weller RE, Kaas JH. 1981a. The organization of somatosensory area II in tree shrews. J Comp Neurol 201:121–133.

Sur M, Weller RE, Kaas JH. 1981b. Physiological and anatomical evidence for a discontinuous representation of the trunk in S-I of tree shrews. J Comp Neurol 201:135–147.

Swanson L. 2003. Brain maps: structure of the rat brain. San Diego: Academic Press.

Tootell RB, Silverman MS, De Valois RL, Jacobs GH. 1983. Functional organization of the second cortical visual area in primates. Science 220:737–739.

Usrey WM, Muly EC, Fitzpatrick D. 1992. Lateral geniculate projections to the superficial layers of visual cortex in the tree shrew. J Comp Neurol 319:159–171.

Uylings HB, Groenewegen HJ, Kolb B. 2003. Do rats have a prefrontal cortex? Behav Brain Res 146:3–17.

Valente T, Auladell C, Perez-Clausell J. 2002. Postnatal development of zinc-rich terminal fields in the brain of the rat. Exp Neurol 174:215–229.

Van Brederode JF, Mulligan KA, Hendrickson AE. 1990. Calcium-Binding proteins as markers for subpopulations of gabaergic neurons in monkey striate cortex. J Comp Neurol 298:1–22.

Van Hooser SD, Heimel JA, Chung S, Nelson SB, Toth LJ. 2005. Orientation selectivity without orientation maps in visual cortex of a highly visual mammal. J Neurosci 25:19–28.

Vogt BA, Miller MW. 1983. Cortical connections between rat cingulate cortex and visual, motor, and postsubicular cortices. J Comp Neurol 216:192–210.

Vogt BA, Peters A. 1981. Form and distribution of neurons in rat cingulate cortex: areas 32, 24, and 29. J Comp Neurol 195: 603–625.

Vogt BA, Vogt L, Farber NB. 2004. Cingulate cortex and disease models. In: Paxinos G, editor. The rat nervous system. London: Elsevier, p 704–727.

von Bonin G, Bailey P. 1961. Pattern of the cerebral isocortex. In: Hofer H, Schultz AH, Starck D, eds. Primatologia, Handbook of Primatology. Basel: Karger, 10:1–42.

Walker C, Sinha MM. 1972. Somatotopic organization of smll cerebral neocortex in albino rat. Brain Res 37:132–136.

Wang Q, Burkhalter A. 2007. Area map of mouse visual cortex. J Comp Neurol 502:339–357.

Wang Y, Kurata K. 1998. Quantitative analyses of thalamic and cortical origins of neurons projecting to the rostral and caudal forelimb motor areas in the cerebral cortex of rats. Brain Res 781: 135–147.

Wassle H, Regus-Leidig H, Haverkamp S. 2006. Expression of the vesicular glutamate transporter VGluT2 in a subset of cones of the mouse retina. J Comp Neurol 496:544–555.

Weber JT, Huerta MF, Kaas JH, Harting JK. 1983. The projections of the lateral geniculate nucleus of the squirrel monkey: studies of the interlaminar zones and the S layers. J Comp Neurol 213: 135–145.

Weller RE, Sur M, Kaas JH. 1987. Callosal and ipsilateral cortical connections of the body surface representations in SI and SII of tree shrews. Somatosens Res 5:107–133.

Wise SP. 1985. The primate premotor cortex: past, present, and preparatory. Annu Rev Neurosci 8:1–19.

Wise SP, Donoghue JP. 1986. Motor cortex of rodents. New York: Plenum.

Wong P, Gharbawie OA, Luethke LE, Kaas JH. 2008. Thalamic connections of architectonic subdivisions of temporal cortex in grey squirrels (*Sciurus carolinensis*). J Comp Neurol 510:440–461.

Wong P, Kaas JH. 2008. Architectonic subdivisions of neocortex in the gray squirrel (*Sciurus carolinensis*). Anat Rec (Hoboken) 291: 1301–1333.

Wong-Riley M. 1979. Changes in the visual system of monocularly sutured or enucleated cats demonstrable with cytochrome oxidase histochemistry. Brain Res 171:11–28.

Wong-Riley MT, Norton TT. 1988. Histochemical localization of cytochrome oxidase activity in the visual system of the tree shrew: normal patterns and the effect of retinal impulse blockage. J Comp Neurol 272:562–578.

Wu CW, Bichot NP, Kaas JH. 2000. Converging evidence from microstimulation, architecture, and connections for multiple motor areas in the frontal and cingulate cortex of prosimian primates. J Comp Neurol 423:140–177.

Wu CW, Kaas JH. 2003. Somatosensory cortex of prosimian galagos: physiological recording, cytoarchitecture, and corticocortical connections of anterior parietal cortex and cortex of the lateral sulcus. J Comp Neurol 457:263–292.

Zilles K. 1978. A quantitative approach to cytoarchitectonics. I. The areal pattern of the cortex of *Tupaia belangeri*. Anat Embryol 153:195–212.

Zilles K. 1990. Organization of the neocortex. In: Tees B, Kolb RC, editors. The cerebral cortex of the rat. Cambridge, MA: MIT Press, p 21–34.

Zilles K. 2004. Architecture of the human cerebral cortex. In: Paxinos G, Mai J, editors. The human nervous system. Amsterdam: Elsevier. p 997–1055.

Zilles K, Wree A. 1995. Cortex: areal and laminar structure. Sydney: Academic Press.